

How Safe Will I Be Given What I Saw? Calibrated Safety Prediction for Image-Controlled Autonomy

Zhenjiang Mao^{1*}, Mrinall Eashaan Umasudhan¹ and Ivan Ruchkin¹

¹Trustworthy Engineered Autonomy (TEA) Lab, University of Florida, Gainesville, FL, USA.

*Corresponding author(s). E-mail(s): z.mao@ufl.edu;

Abstract

Autonomous robots that rely on deep neural network controllers pose critical challenges for safety prediction, especially under partial observability and distribution shift. Traditional model-based verification techniques are limited in scalability and require access to low-dimensional state models, while model-free methods often lack reliability guarantees. This paper addresses these limitations by introducing a framework for calibrated safety prediction in end-to-end vision-controlled systems, where neither the state-transition model nor the observation model is accessible. Building on the foundation of world models, we leverage variational autoencoders and recurrent predictors to forecast future latent trajectories from raw image sequences and estimate the probability of satisfying safety properties. We distinguish between monolithic and composite prediction pipelines and introduce a calibration mechanism to quantify prediction confidence. In long-horizon predictions from high-dimensional observations, the forecasted inputs to the safety evaluator can deviate significantly from the training distribution due to compounding prediction errors and changing environmental conditions, leading to miscalibrated risk estimates. To address this, we incorporate unsupervised domain adaptation to ensure robustness of safety evaluation under distribution shift in predictions without requiring manual labels. Our formulation provides theoretical calibration guarantees and supports practical evaluation across long prediction horizons. Experimental results on three benchmarks — racing car, cart pole, and donkey car — show that our UDA-equipped evaluators maintain high accuracy and substantially lower false positive rates under distribution shift. Similarly, world model-based composite predictors outperform their monolithic counterparts on long-horizon tasks, and our conformal calibration provides reliable statistical bounds.

Keywords: Pixel-to-action control, world models, confidence calibration, conformal prediction, unsupervised domain adaptation

1 Introduction

Autonomous robots increasingly rely on high-resolution sensors (e.g., cameras, lidars) and deep-learning architectures [1–3]. End-to-end reinforcement and imitation learning have become widespread, bypassing traditional components such as state estimation and planning [4–6]. Although effective, these end-to-end systems often depend on complex, opaque models whose internal decision-making processes are difficult to interpret [7]. This lack of transparency, combined with the inherent variability and unpredictability of real-world conditions, makes it difficult to anticipate potential failures before they manifest [8, 9]. Failures in autonomous driving can lead to catastrophic accidents, which erode public trust and hinder broader adoption [10]. Robust safety prediction is therefore essential to ensure the reliability and acceptance of these systems, making it both a technical hurdle and a societal imperative.

In the autonomous driving industry, vision-based frameworks such as Tesla Vision demonstrate the feasibility of end-to-end control using only camera inputs [11]. By learning scene geometry and motion directly from raw images, such systems remove map and sensor dependencies and adapt more readily to new roads and dynamic conditions. However, this image-only paradigm amplifies the need for robust, well-calibrated safety prediction, as perception and control are fully integrated and lack explicit, low-dimensional state representations.

Moreover, in safety-critical settings, quantifying uncertainty becomes essential to operate under partial observability or environmental variability. However, modern deep models often produce overconfident or miscalibrated outputs, undermining reliability [12, 13]. In autonomous robots, this can result in unsafe behavior or missed interventions [14, 15]. Thus, to ensure safety, predictions must be accompanied by confidence estimates that accurately reflect real-world outcomes.

Many existing safety prediction methods depend on low-dimensional, physically meaningful states (e.g., poses and velocities) and hand-crafted indicators that require extensive domain knowledge and offline analysis, making them impractical for online application to high-dimensional, image-based controllers [16–19]. Additionally, model-based offline verification scales poorly to vision systems, as it demands detailed modeling of the perception subsystem [20–22]. Similarly, black-box statistical risk assessments still tend to assume low-dimensional state representations and rich outcome labels (e.g., signal robustness) [23–25]. Recent graph-based models HDGT, FutureNet, and SemanticFormer represent the road environment as a graph whose nodes correspond to map elements (e.g., lanes, intersections) and dynamic agents, and whose edges encode spatial or temporal relationships [26–28]. These models use the graph structure to perform multi-agent trajectory prediction conditioned on HD maps, precomputed lane graphs, and multiple sensors inputs. This dependence incurs high annotation and maintenance costs and limits application to unmapped or rapidly changing environments.

However, purely data-driven, image-based predictors themselves can suffer under distribution shift, leading to miscalibrated risk estimates and degraded accuracy when encountering novel environmental conditions [9, 29]. Under these circumstances, the predicted vision trajectory cannot be accurately classified by a visual safety evaluator,

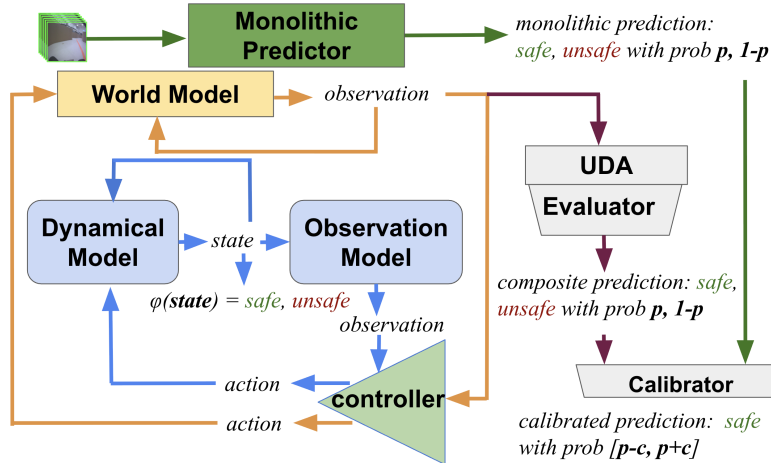


Fig. 1 Safety prediction pipelines for image-controlled autonomous systems. The **blue arrows** represent the underlying dynamics loop, consisting of the unknown dynamical model, unknown observation model, and known controller. The **orange arrows** indicate the learned *world model loop*, where future observations are simulated based on past observations and actions. The **green path** illustrates the *monolithic prediction pipeline*, which directly predicts safety outcomes (safe/unsafe with probability p) from observations. The **purple path** shows the *composite prediction pipeline*, where a forecaster predicts future observations that are passed to a safety evaluator.

where the small errors compound over time, producing visual trajectories whose distribution deviates substantially from the training data. As a result, a static evaluator trained offline often fails to maintain calibration and exhibits inflated false-positive rates, which directly undermines reliability in safety-critical decisions. This motivates the need for an adaptive mechanism that can align the evaluator to the evolving input distribution without manual relabeling [30].

This article addresses the problem of **reliable online safety prediction** without access to a known, low-dimensional dynamical state. Instead, our predictor relies on a rolling window of images, for example, the RGB frames from the most recent m time steps of a race car’s run. Given this image history, our goal is to predict the probability that the car will stay on track for the next k frames. We also require that this predicted probability is *calibrated well*; that is, the events forecast with probability p should occur approximately a p fraction of the time.

We introduce a flexible family of learning pipelines, shown in Figure 1, for image-based safety prediction, featuring: (i) *deep world models* that learn compact latent representations from raw observations and jointly model the dynamics to predict future observations; (ii) monolithic models that *capture temporal evolution* of latent safety-critical features without reconstructing full observations; (iii) an *adaptive UDA module* that detects distribution shifts and selectively fine-tunes the safety evaluator online to maintain calibration on shifted inputs and (iv) *post-hoc conformal calibration method* that converts raw scores into trustworthy probabilities independently of the underlying architecture.

We evaluate our pipeline on three benchmarks of long-horizon safety prediction: racing car and cart pole from simulated OpenAI Gym environments and a physical deployment of camera-driven racing cars, known as Donkey Cars [31, 32]. Our results reveal the advantages of modular pipelines with attention mechanisms and show that predicting calibrated probabilities is easier than predicting binary safety labels over extended horizons.

In summary, this article makes three contributions:

1. A family of *modular pipelines for safety prediction* in image-controlled autonomous robots.
2. A *conformal post-hoc calibration* technique to equip safety estimates with statistical guarantees.
3. A *comprehensive, realistic experimental evaluation* that highlights the impact of modularity and calibration on long-horizon safety prediction.

An earlier iteration of this work appeared in a conference paper [30]. This journal article substantially extends the conference version in three key ways:

1. We develop a UDA method for making safety evaluators robust to distribution shift. In addition to our original image-based evaluator, we introduce a novel *latent-space safety evaluator*, enabling more robust post-hoc safety estimation for forecasted visual observations and latent states.
2. We improve the long-horizon performance of our pipelines with the latest world-model architectures: bidirectional LSTMs, Vector Quantized VAEs (VQ-VAEs), and Transformers.
3. We introduce a new physical case study of vision-based Donkey Cars to evaluate our predictors on a realistic high-speed autonomous racing.

2 Related Work

2.1 Trajectory Prediction

A common way of predicting the system’s performance and safety is by inferring it from *predicted trajectories*. Classic approaches consider model-based prediction, for instance, estimating collision risk with bicycle dynamics and Kalman filtering [33, 34]. One common approach with safety guarantees is *Hamilton-Jacobi* (HJ) reachability, which requires precomputation based on a dynamical model [35, 36]. Among many deep learning-based predictors, a popular architecture is *Trajectron++*, which takes in high-dimensional scene graphs and outputs future trajectories for multiple agents [37, 38]. A conditional VAE is adopted in Trajectron++ to add constraints at the decoding stage [39]. This can predict more than one reasonable trajectory option under the encoding condition, which helps analyze the future safety under different ego-vehicle intentions. Learning-based trajectory predictions can be augmented with conformal prediction to improve their reliability [25, 40]. These techniques have also been adapted to motion planning settings, where adaptive conformal prediction provides calibrated guarantees for multi-agent collision avoidance [41]. Recent work

has further emphasized generalizability and interpretability as key desiderata for trajectory predictors, advocating for Bayesian latent-variable models to provide better uncertainty modeling and extrapolation across scenarios [42].

In comparison, our work eschews handcrafted scene and state representations, instead using image and latent representations that are informed by safety. This trend is echoed in efforts to design self-aware and interpretable neural networks [43] for robust trajectory prediction under uncertainty and interpretable world models using physically meaningful representations under dynamical constraints [44, 45].

2.2 Performance and Safety Evaluation

A variety of recent research enables robotic systems to *self-evaluate* their competency [46]. Performance metrics vary significantly and include such examples as the time to navigate to a goal location or whether a safety constraint was violated, which is the focus of our paper. For systems that have access to their low-dimensional state, such as the velocity and the distance from the goal, *hand-crafted indicators* have been successful in measuring performance degradation. These indicators have been referred to robot vitals, alignment checkers, assumption monitors, and operator trust [18, 47–49]. Typically, these indicators rely on domain knowledge and careful offline analysis of the robotic system, which are difficult to respectively obtain and perform for high-dimensional sensors.

Deep neural network (DNN) controllers are particularly vulnerable to distribution shift and difficult to formally analyze [50, 51]. This challenge, combined with the critical need for safety and performance guarantees, has driven the development of both model-based and model-free prediction approaches. On the model-based side, *closed-loop verification approaches* perform reachability analysis to evaluate the safety of a DNN-controlled system [52, 53]; however, when applied to vision-based systems, these techniques require detailed modeling of the vision subsystem and have limited scalability [22, 54, 55]. Furthermore, these closed-loop verification methods fundamentally require an explicit low-dimensional dynamical model to perform reachability analysis; our framework operates end-to-end from image sequences to safety predictions without access to such a model, making these methods architecturally incompatible with our setting [52, 53]. On the other hand, *model-free safety predictions* rely on the correlation between performance and uncertainty measures/anomaly scores, such as autoencoder reconstruction errors and distances to representative training data [56]. Striking the balance between model-based and model-free approaches are *black-box statistical methods* for risk assessment and safety verification [57–60], such as uncertainty quantification with statistical guarantees in end-to-end vision-based control [60]. These methods require low-dimensional states and rich outcome labels (such as signal robustness) — an assumption that we are relaxing in this work while addressing a similar problem.

In addition, safe planning and control solve a problem complementary to ours: they find actions to control a robot safely, usually with respect to a dynamical model, such as motion planning under uncertainty for uncertain systems and a growing body of work on control barrier functions [61–65]. Some approaches are robust to measurement errors induced by learning-based perception, but at their core, they still

hinge on the utilization of low-dimensional states, a paradigm we aim to circumvent entirely [66, 67]. Importantly, one of our constraints is assuming the existence of an end-to-end controller (possibly implemented with the above methods), with no room for modifications.

In the context of confidence calibration, the softmax scores of classification neural networks can be interpreted as probabilities for each class; however, standard training leads to miscalibrated neural networks, as measured by *Brier score* and *Expected Calibration Error* (ECE) [12, 13]. Calibration approaches can be categorized into *extrinsic (post-hoc) calibration* added on top of a trained network, such as Platt and temperature scaling, isotonic regression, and histogram/Bayesian binning—and *intrinsic calibration* to modify the training, such as ensembles, adversarial training, and learning from hints, error distances, or true class probabilities [12, 68–75]. Similar techniques have been developed for calibrated regression [76, 77]. It is feasible to obtain calibration guarantees for safety chance predictions, but it requires a low-dimensional model-based setting [18, 78]. While recent work focuses on conformal calibration of temporal logic satisfaction in structured, model-based systems, our work addresses a different challenge: calibrating safety chance predictions directly from image sequences in end-to-end controlled systems without access to low-dimensional state or explicit logical specifications [25]. To the best of the authors’ knowledge, such guarantees have not been instantiated in a model-free autonomy setting.

2.3 World Models

For systems with high-resolution images and complex dynamical models, trajectory prediction becomes particularly challenging. Physics-based methods and classical machine learning methods may not be applicable to these tasks, leading to the almost exclusive application of deep learning for prediction. *Sequence prediction models*, which originate in deep video prediction, often struggle in our setting due to compounding prediction errors, the difficulty of modeling long-term dependencies, and the large data requirements for learning high-dimensional dynamics [79]. However, incorporating additional information, such as states, observations, and actions, in sequence predictions can improve their performance — and our predictors take advantage of that [80–82]. Another way to improve performance is to reduce the input dimensionality. High-dimensional sensor data often contains substantial redundant and irrelevant information, which leads to higher computational costs. Generative adversarial networks (GANs) map the observations into a low-dimensional latent space, which can enable model-based assurance algorithms, and low-dimensional representations can incorporate conformal predictions to monitor the real-time performance [83–85]. *World models* [86] are a model-based approach in which a learned environment model serves as a surrogate for the real environment, allowing the controller to be trained largely in imagination rather than through direct interaction with the physical world. This can substantially improve sample efficiency and stability compared to training solely in the real environment. They achieve better results in training the controllers than basic RL. The world model learns an approximation of the system’s dynamics by collecting observations and actions as inputs and outputs the future states. The observation encoder, typically implemented as a VAE, compresses each observation into

a latent space (low-dimensional vectors) and trains a mixed-density recurrent neural network (MDN-RNN) to forecast the next-step latent observations. The decoder of the VAE maps the latent vector into the observation space. This VAE-MDN-RNN world model is then applied to do trajectory predictions and get the competency assessment through the forecasting trajectory [87].

Recent advances explore the use of discrete latent spaces for more structured and sample-efficient planning, including transformer-based discrete world models for continuous control, building on neural discrete representation learning and echoing our use of VQVAE-based encoders [88, 89]. Building on the original VAE-MDN-RNN architecture of world models, more advanced models like *DreamerV2* and *IRIS* adopt recent deep computer vision models like vision transformers to achieve more vivid images [86, 90, 91]. Transformers have also been shown to improve sample efficiency in latent model training, a crucial factor for model-based planning and control [92]. Recent systems such as DayDreamer extend this line of work by leveraging compact world models for sample-efficient control in physical robots, demonstrating the practicality of Dreamer-style pipelines [93]. More recently, Orbis compares different latent spaces within a unified hybrid tokenizer, showing that a flow-matching-based continuous model achieves superior long-horizon prediction in challenging driving scenarios using only raw video data [94].

The trajectories predicted by world models have been used to provide uncertainty measurements for agents, albeit without statistical guarantees so far [95]. In our method, we adopt different architectures of world models and compare them with other one-step monolithic deep learning models using the recurrent modules. Building on this foundation, recent work has demonstrated that pre-trained, interpretable world models can enable zero-shot safety prediction from visual inputs, and that weakly supervised latent representations can further improve physical consistency and trajectory-level accuracy [45, 96]. These efforts are aligned with emerging principles for physically interpretable world models, which call for organized latent spaces, aligned invariant/equivariant representations, integration of diverse supervision, and partitioned outputs for scalability [44]. Compared with these approaches, this article develops chance calibration guarantees, which were previously unexplored.

2.4 Unsupervised Domain Adaptation

Predicting future observations from high-dimensional sensory inputs, such as image sequences, inevitably leads to distribution shift, especially over long prediction horizons. This shift may arise from subtle environmental variations, motion blur, sensor noise, or compounding prediction errors. When applied to such shifted predictions, safety evaluators often produce unreliable or overconfident outputs, which compromise downstream decision-making [29, 97]. To address this, we adopt a principled solution of *unsupervised domain adaptation (UDA)* that continuously adapts the safety evaluator to the evolving input distribution without requiring manual relabeling. This enables the system to maintain calibration guarantees even as the environment changes or predictions drift from training conditions.

A range of UDA strategies has been developed across machine learning and robotics. Early methods, such as Deep CORAL and MMD-based alignment, align

source and target feature distributions via statistical matching [98, 99]. Adversarial approaches like DANN and ADDA train domain-invariant representations by using domain discriminators [100, 101]. Others operate at the image level using GAN-based transformations [102–104]. More recent work enables adaptation at test time, including entropy-based methods like Tent and contrastive self-supervised approaches such as CoSCA [105, 106]. In our work, we adopt a lightweight method using the entropy minimization (MEMO) approach, which does not require source data during adaptation [107]. It is well-suited for safety evaluation in long-horizon prediction settings because it can be applied efficiently within the prediction pipeline without querying external data.

3 Background and Problem

This section introduces the necessary notation and describes the problem addressed in this article.

3.1 Problem Setting

Definition 1 (Robotic system) A discrete-time *robotic system* $s = (\mathbf{X}, \mathbf{Y}, \mathbf{U}, h, f, o, x_0, \varphi)$ consists of:

- *State space* \mathbf{X} , containing continuous states x
- *Observation space* \mathbf{Y} , containing images y
- *Action space* \mathbf{U} , with commands u
- *Image-based controller* $h : \mathbf{Y} \rightarrow \mathbf{U}$, typically implemented by a neural network
- *Dynamical model* $f : \mathbf{X} \times \mathbf{U} \rightarrow \mathbf{X}$, determines the next state (unknown to us)
- *Observation model* $o : \mathbf{X} \rightarrow \mathbf{Y}$, which generates an observation based on the state (unknown to us)
- *Initial state* x_0 , from which the system starts executing
- *State-based safety property* $\varphi : \mathbf{X} \rightarrow \{0, 1\}$, which determines whether a given state x is safe

We focus on robotic systems with observation spaces with thousands of pixels and unknown non-linear dynamical and observation models. In such systems, while the state space \mathbf{X} is conceptually known (if only to define φ), it is not necessary (and often difficult) to construct f and o because the controller acts directly on the observation space \mathbf{Y} . Without relying on f and o , end-to-end methods like deep reinforcement learning and imitation learning are used to train a controller h by using data from the observation space [108, 109]. Once the controller is deployed in state x_0 , the system executes a *trajectory*, which is a sequence $\{x_i, y_i, u_i\}_{i=0}^t$ up to time t , where:

$$x_{i+1} = f(x_i, u_i), \quad y_i = o(x_i), \quad u_i = h(y_i) \tag{1}$$

We consider robotic systems where the underlying dynamical model f and observation model o are unknown. This means we cannot explicitly use the known dynamical

and observation models to predict future safety. Instead, we extract predictive information from three sources of data. First, we will use the current observation, y_i , at some time i . For example, when a car is at the edge of the track, it has a higher probability of being unsafe in the next few steps. Second, past observations y_{i-m+1}, \dots, y_i provide dynamically useful information that can only be extracted from time series, such as the speed and direction of motion. For example, just before a car enters a turn, the sequence of past observations implicitly informs how hard it will need to be to remain safe. Third, not only do observations inform safety, but so do the controller’s past/present outputs $h(y_{i-m+1}, \dots, y_i)$. For instance, if by mid-turn the controller has not changed the steering angle, it may be less likely to navigate this turn safely. In addition, forecasting future control actions $(\hat{u}_{i+1}, \dots, \hat{u}_{i+k})$ would provide another input to predict the trajectory.

Our goal is to predict the system’s safety $\varphi(x_{i+k})$ at time $i+k$ given a series of m observations $\mathbf{y}_i = (y_{i-m+1}, \dots, y_i)$. This sequence of observations does not, generally, determine the true state x_i (e.g., when $m = 1$, the function o may not be invertible). This leads to *partial state observability*, which we model stochastically. Specifically, we say that from the predictor’s perspective, x_i is drawn from some belief distribution $\mathcal{D}_{\mathbf{y}_i}$. This induces a distribution of subsequent trajectories and transforms future safety $\varphi(x_{i+k})$ into a Bernoulli random variable. Therefore, we will estimate the conditional probability $P(\varphi(x_{i+k}) \mid \mathbf{y}_i)$ and provide an error bound on our estimates. Note that process noise in d and measurement noise in o are both supported by our approach and would be treated as part of the stochastic uncertainty in the future φ . To sum up the above, we arrive at the following problem description.

Problem 1 (Calibrated safety prediction) Given horizon $k > 0$, confidence $\alpha \in (0, 0.5)$, and observations \mathbf{y}_i from some system s with unknown f and o , estimate future safety chance $P(\varphi(x_{i+k}) \mid \mathbf{y}_i)$ and provide an upper bound for the estimation error that holds for at least $1 - \alpha\%$ of estimates.

In addition, instead of only outputting an estimated safety chance, we aim to provide a guaranteed interval around it.

Problem 2 (Probability interval prediction) Given the same inputs as Problem 1 and an estimate $P'(\varphi(x_{i+k}) \mid \mathbf{y}_i)$ from a safety chance predictor, determine an interval over the estimated confidence with width c such that it contains the true chance $P(\varphi(x_{i+k}) \mid \mathbf{y}_i)$ with confidence α :

$$\mathbb{P}\left(\left|P'(\varphi(x_{i+k}) \mid \mathbf{y}_i) - P(\varphi(x_{i+k}) \mid \mathbf{y}_i)\right| \leq c\right) \geq 1 - \alpha.$$

3.2 Predictors and Datasets

To address our problem, we consider two types of safety predictors: one that outputs a binary safety label, and another that outputs the probability of being safe in the future.

Definition 2 (Safety label predictor) For horizon $k > 0$, a *safety label predictor* $\rho : \mathbf{Y}^m \rightarrow \{0, 1\}$ predicts the binary safety outcome $\varphi(x_{i+k})$ at time $i + k$.

Definition 3 (Safety chance predictor) For horizon $k > 0$, a *safety chance predictor* $g : \mathbf{Y}^m \rightarrow [0, 1]$ estimates the probability $P'(\varphi(x_{i+k}) \mid \mathbf{y}_i)$ that the system remains safe at time $i + k$.

Definition 4 (Safety chance interval predictor) For horizon $k > 0$, a *safety interval predictor* $\eta : \mathbf{Y}^m \rightarrow [0, 1] \times [0, 1]$ estimates the interval of probabilities $[P'(\varphi(x_{i+k}) \mid \mathbf{y}_i) - c, P'(\varphi(x_{i+k}) \mid \mathbf{y}_i) + c]$ that the system remains safe at time $i + k$ such that the true probability $P(\varphi(x_{i+k}) \mid \mathbf{y}_i)$ lies within that interval with confidence at least $1 - \alpha$, where $\alpha \in (0, 0.5)$.

Both types of predictors are trained using labeled *observation-action datasets*, which combine each observation with the controller’s executed action and the eventual safety label. This setup enables training without sacrificing predictive fidelity, as actions encode critical behavioral information even in visually ambiguous settings. Thus, all models described in this article are trained on datasets of the following form:

Definition 5 (Observation-action dataset) An *observation-action dataset* $\mathbf{Z} = \{(\mathbf{z}_j, \varphi_j) \mid j = 1, \dots, N\}$ consists of m -length sequences of image-action pairs

$$\mathbf{z}_j = ((y_{i-m+1}, u_{i-m+1}), \dots, (y_i, u_i))$$

and a safety label $\varphi_j := \varphi(x_{i+k})$ obtained k steps later.

Notice that our dataset is structured not around sequential states within a single trajectory, but as independent trajectories sampled from the same distribution. This ensures that the calibration and test samples are i.i.d., satisfying the exchangeability requirement of conformal prediction. We are not applying conformal prediction to temporally correlated states along a single trajectory; rather, each data point represents an independent realization of the same prediction task.

4 Modular Family of Safety Predictors

We begin by describing the construction of *safety-label predictors* and then show how they are upgraded to *safety-chance predictors* that quantify uncertainty.

4.1 Monolithic and Composite Predictors

Our family of safety predictors rests on a simple modularity principle: any safety-label predictor can be decomposed into three conceptually independent blocks that communicate through a latent space Θ . An *encoder* E maps each observation $y_i \in \mathcal{Y}$ to a latent state $\theta_i \in \Theta$. A *forecaster* P is a generic sequence operator that consumes a window of past states and returns a forecast k steps ahead; its internal mechanism is not fixed: it can be recurrent, convolutional, attentional, or something else entirely.

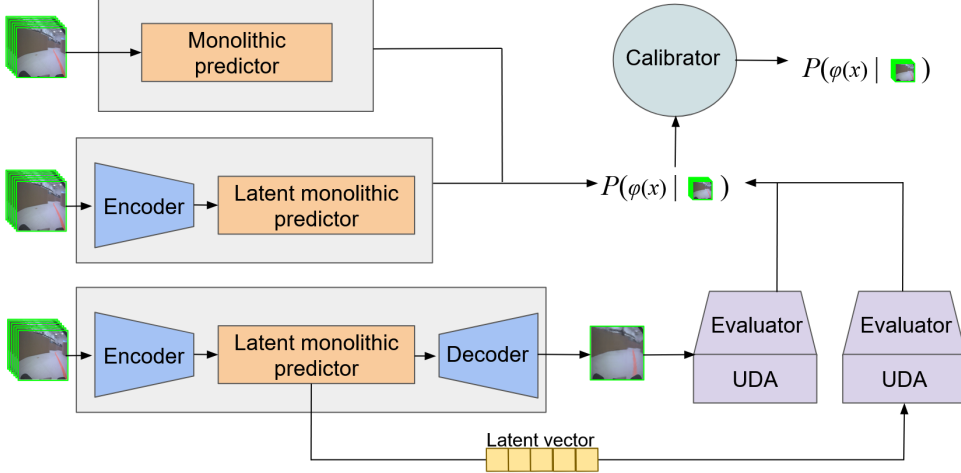


Fig. 2 Comparison of safety prediction pipelines and their world-model structures (gray boxes). **Top:** The *monolithic predictor* maps image sequences directly to safety probabilities $P(\varphi(x))$, followed by a *calibrator* for improved confidence. **Middle:** The *latent monolithic predictor* encodes images into latent states and predicts safety from these, with calibration applied afterward. **Bottom:** The *composite latent predictor* encodes inputs, forecasts future latent states, and uses an *evaluator* with UDA to estimate safety. All pipelines predict the probability of satisfying the safety property $\varphi(x)$.

Finally, an *evaluator* V assigns a binary safety label to the forecast. Similar to the predictor, its internal mechanism is not fixed.

Since P is abstract, the same modular decomposition and reasoning apply whether it is implemented as an LSTM, a GRU, a temporal convolution, a Transformer encoder stack, or any future architecture with the requisite input–output signature. In what follows, we treat P entirely as a black box. The only place we commit to a concrete realisation is in the experimental section, where we provide numerical results for two instantiations — an LSTM and a Transformer — chosen to illustrate, respectively, recurrence and attention.

Two architectural designs arise from our modular view. A *monolithic* predictor applies the encoder E and immediately feeds its latent output to the evaluator V , so the safety label is produced in a single forward pass with no separate forecasting block. A *composite* predictor inserts an explicit forecasting stage: it first reconstructs a sequence of latent states and then feeds those predictions to V for evaluation. Figures 1 and 2 illustrate both dataflows.

Definition 6 (Monolithic latent predictor) Let $E : \mathcal{Y} \rightarrow \Theta$ be an encoder and $V : \Theta \rightarrow \{0, 1\}$ an evaluator. The composition $g = V \circ E$ is called a *monolithic latent predictor*.

Composite pipelines explicitly separate forecasting from evaluation. In the image space, a forecaster P_g predicts future frames that are then classified by a CNN. In

the latent space, a forecaster P_l outputs $(\theta'_{i+1}, \dots, \theta'_{i+k})$, after which V inspects the latent trajectory. Similarly, the design of the composite pipeline does not restrict how the forecaster is built; it may rely on recurrence, attention, or any hybrid thereof.

Definition 7 (Composite image predictor) A composite image predictor comprises two learned modules: (i) an *image forecaster* $P_g : \mathcal{Z}_m \rightarrow \mathcal{Y}$ that maps the past m observations z_i to a forecasted image \hat{y}_{i+k} , and (ii) an *evaluator* $V : \mathcal{Y} \rightarrow \{0, 1\}$ that assigns a binary safety label to each predicted image. The overall prediction is

$$g(z_i) = V(F_g(z_i)).$$

Definition 8 (Composite latent predictor) A composite latent predictor consists of three learned modules: (i) an *encoder* $E : \mathcal{Z} \rightarrow \Theta$ that maps each observation z_i to a latent state $\theta_i \in \Theta$; (ii) a *latent forecaster*

$$P_l : \underbrace{\Theta \times \dots \times \Theta}_m \longrightarrow \underbrace{\Theta \times \dots \times \Theta}_n$$

m past states n predicted states

that, given $(\theta_{i-m+1}, \dots, \theta_i)$, produces the sequence $(\hat{\theta}_{i+k-n+1}, \dots, \hat{\theta}_{i+k})$; and (iii) an *evaluator* $V : \Theta \rightarrow \{0, 1\}$ that labels each predicted state. Thus, the composite prediction is denoted as

$$V(\hat{\theta}_{i+k-n+1}, \dots, \hat{\theta}_{i+k}).$$

For the latent forecaster P_l , we compare three architectures. The first is a unidirectional LSTM, which provides a strong recurrent baseline. The second extends this with a bidirectional LSTM that incorporates a backward pass, allowing predictions during training to condition on both preceding and succeeding elements of the input sequence [110]. This enables the model to construct richer temporal representations with enhanced coherence and accuracy of the forecasted output window. Lastly, we adopt a Transformer-based architecture in which each layer combines multi-head self-attention with a position-wise feed-forward network, connected via residual links and layer normalization [111]. This design allows every time step in the input window to attend to all others within the same window, enabling the model to capture complex long-range dependencies more effectively than recurrent models. Once the forecast $(\hat{\theta}_{i+k-n+1}, \dots, \hat{\theta}_{i+k})$ is produced, the evaluator V emits only a single binary label and does not benefit from future context; therefore, we implement V as a lightweight unidirectional LSTM, which is both parameter-efficient and sufficient for this one-step task.

In the composite latent predictor pipeline, in addition to the standard continuous-latent VAE encoder, we also evaluate a discrete-latent variant based on the Vector Quantized VAE (VQ-VAE) architecture [89]. The VQ-VAE maps each observation into a sequence of discrete codes drawn from a learned codebook, which serves as a compact, structured representation of the input. This comparison allows us to assess whether discrete latent representations offer improved stability and safety-prediction accuracy in the composite pipeline.

4.2 Training Process

Monolithic predictors g , evaluators V , and image forecasters P_g are trained in a supervised manner on a training dataset Z_{tr} containing observation sequences with associated safety labels or future images, respectively. For the composite models, we adopt a two-stage training procedure. First, the VAE encoder E is trained (as described in the next paragraph) to produce latent representations of observations. Then, the latent forecasters P_l are trained on future latent vectors, obtained from true future observations with a VAE encoder E . The *mean squared error (MSE)* loss is implemented for the LSTM and Transformer latent forecasters, since the MSE loss directly penalizes deviations between predicted and true continuous latent vectors. The monolithic predictors and evaluators use *cross-entropy (CE)* as the loss function, whereas it is suited for classification tasks like safety evaluation, as it maximizes the probability of the correct class. We also implement an early stopping strategy to reduce the learning rate as the loss drop slows down — if the average loss improvement over the past 10 consecutive epochs is smaller than 10^{-4} , we stop the training. Additionally, the learning rate is reduced when the loss drop slows down to encourage finer convergence.

For the VAE, the total loss L consists of two parts. The first is the reconstruction loss L_{recon} , which quantifies how well an original image y is approximated by $d(e(y))$ using the MSE loss. The second is the latent loss L_{latent} , which uses the Kullback–Leibler divergence loss to minimize the difference between two latent-vector probability distributions $e(y | \theta) \approx d(\theta | y)$, where θ is a latent vector and y is an input. Thus, the total loss function for the VAE combines the three parts with a regularization parameter $\lambda_1 > 0$:

$$L = L_{\text{recon}} + \lambda_1 L_{\text{latent}} \quad (2)$$

One challenge is that the safety label balance changes in Z_{tr} with the prediction horizon k , leading to imbalanced data for higher horizons. To ensure a balanced label distribution, we resample with replacement for a 1:1 safe:unsafe class balance in the training data.

4.3 Unsupervised Domain Adaptation

The forecasts of latent vectors and observations in a composite pipeline are likely to be distribution-shifted, illustrated in Figure 3. Such shifts degrade the accuracy of the safety evaluator. Since safety-labeling a significant amount of such data is impractical, we employ an *unsupervised domain adaptation* strategy at test time to mitigate the impact on the evaluator accuracy without *any* additional labels.

We adopt the *Marginal Entropy Minimization* (MEMO) approach for per-sample test-time adaptation [107]. The key idea is to encourage the evaluator to produce confident and consistent predictions across multiple stochastically augmented versions of the same observation. This is achieved by: (1) generating augmented versions of the input visual observations; (2) aggregating their predictions into a marginal probability distribution; and (3) minimizing the entropy of this marginal distribution by updating the evaluator parameters.

Algorithm 1 Conformal calibration for chance predictions

Require: A validation dataset bin $B = \{b_k\}_{k=1,\dots}$, each containing sequences of observations and safety $b_k = (y_k, \phi(x_k))$, trained safety chance predictor g , and miscoverage level α

Ensure: confidence bound c satisfying Equation. 4.

```
1: Function ConCali( $B, g, \alpha$ ):
2:   for  $j = 1$  to  $Q$  do
3:     for  $i = 1$  to  $M$  do
4:        $B_i \leftarrow N$  i.i.d. samples from  $B$  {resampled bin}
5:        $q_i \leftarrow \frac{1}{N} \sum_{l=1}^N g(y_l)$ , for each  $y_l \in B_i$  {mean safety chance prediction}
6:        $p_i \leftarrow \frac{1}{N} \sum_{l=1}^N \phi(x_l)$ , for each  $\phi(x_l) \in B_i$  {true safety chance}
7:        $\delta_i \leftarrow |q_i - p_i|$  {non-conformity score}
8:     end for
9:      $n \leftarrow \lceil (M + 1)(1 - \alpha) \rceil$  {conformal quantile}
10:     $c \leftarrow$  the  $n$ -th smallest value among  $\{\delta_1, \dots, \delta_M\}$ 
11:  end for
12: return  $c$ 
```

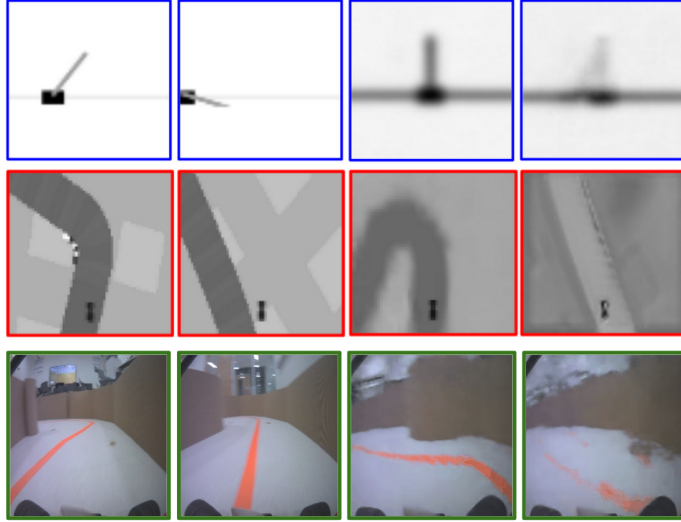


Fig. 3 From top to bottom are the observations of our three cases (top to bottom: cart pole, racing car, and donkey car). The columns (left to right) are safe observation from \mathbf{Y} , unsafe observation from \mathbf{Y} , safe observation from $d(f_l(e(\mathbf{Y})))$, unsafe observation from $f_g(\mathbf{Y})$ under distribution shift.

Let

$$\mathcal{A} = \{a_1, \dots, a_B\}$$

be a set of stochastic augmentation functions (e.g., random crop, color jitter, Gaussian noise), each mapping an image y to an augmented image $a_i(y)$. For each class $s \in \{0, 1\}$, where 0 denotes *unsafe* and 1 denotes *safe*, we compute the *marginal predicted*

probability:

$$\bar{p}_\theta(s | y) = \frac{1}{B} \sum_{i=1}^B V_\theta(s | a_i(y)). \quad (3)$$

The MEMO loss is the negative entropy of the marginal distribution:

$$L_{\text{MEMO}}(\theta; y) = - \sum_{s \in \{0,1\}} \bar{p}_\theta(s | y) \log \bar{p}_\theta(s | y), \quad (4)$$

where L_{MEMO} encourages the evaluator to make low-entropy, consistent predictions across all augmented views.

The evaluator parameters are adapted with a single gradient descent step:

$$\theta^+ \leftarrow \theta - \eta \cdot \nabla_\theta L_{\text{MEMO}}(\theta; y), \quad (5)$$

where $\eta > 0$ is the adaptation learning rate.

The adapted evaluator V_{θ^+} then outputs the predicted safety label:

$$\hat{s} = \arg \max_{s \in \{0,1\}} V_{\theta^+}(s | y). \quad (6)$$

As indicated in Figures 1 and 2, this label-free, per-sample adaptation improves evaluator robustness under latent distribution shift in composite latent predictors.

It is important to distinguish between two sources of distribution shift in our setting. First, the decoded images produced by the VAE may themselves be out-of-distribution for the safety evaluator, even when the underlying trajectory is in-distribution. This shift occurs because reconstruction artifacts and latent-space forecasting errors introduce visual distortions absent from the original training images. Second, the trajectories themselves may be out-of-distribution, representing scenarios not encountered during training. Our test-time adaptation strategy addresses the first source directly: by encouraging consistent, confident predictions across stochastically augmented views of each decoded image, MEMO makes the evaluator robust to the visual perturbations introduced by the decode and predict pipeline, without requiring any additional safety labels.

To mitigate the impact of distribution shifts occurring at the trajectory level, our framework currently relies on the conformal calibration mechanism described in the following section. When the system encounters a trajectory that significantly deviates from the training distribution, the predicted safety chance $P'(\varphi(x_{i+k})|y_i)$ naturally reflects higher uncertainty, leading to wider conformal intervals that alert the controller to potential unreliability [29].

This robustness can be further augmented by leveraging pre-trained foundation world models and multimodal meaning representations [96, 112]. By utilizing the superior zero-shot generalization of these large-scale models, the safety evaluator can potentially reason about novel maneuvers or environmental geometries not present in the local training set, thereby bridging the gap between training and deployment distributions.

4.4 Conformal Calibration for Chance Predictors

Standard calibration methods operate on binary outcomes (safe/unsafe), which makes it difficult to obtain reliable probability guarantees for rare or noisy events. In our setting, we require guarantees not on single predictions but on average safety probabilities within bins, because the chance predictor outputs a continuous safety probability rather than a binary label. This necessitates bin averaging to obtain meaningful statistics, and motivates our use of adaptive binning combined with conformal prediction.

To turn a label predictor ρ into a chance predictor g , we take its normalized softmax outputs and perform post-hoc calibration [12, 71]. On a held-out calibration dataset Z_{cal} , we hyperparameter-tune over state-of-the-art post-hoc calibration techniques: temperature scaling, logistic calibration, beta calibration, histogram binning, isotonic regression, ensemble of near-isotonic regression (ENIR), and Bayesian binning into quantiles (BBQ) [113].

To evaluate the quality of probability estimates produced by our chance predictors, we consider two standard calibration metrics: *Expected Calibration Error* (ECE) and the *Brier Score* [12, 114]. Let $\hat{p}_i \in [0, 1]$ denote the predicted probability of safety for sample i , and $y_i \in \{0, 1\}$ the corresponding ground truth label. Given n samples and a binning function $\text{bin}(\cdot)$ that assigns predictions to Q disjoint bins, ECE is defined as

$$\text{ECE} = \sum_{j=1}^Q \frac{|B_j|}{n} |\text{acc}(B_j) - \text{conf}(B_j)|, \quad (7)$$

where B_j is the set of samples in bin j , $\text{acc}(B_j) = \frac{1}{|B_j|} \sum_{i \in B_j} \mathbf{1}\{y_i = 1\}$ is the empirical accuracy, and $\text{conf}(B_j) = \frac{1}{|B_j|} \sum_{i \in B_j} \hat{p}_i$ is the mean predicted confidence in the bin.

The Brier Score measures the mean squared error between predicted probabilities and actual outcomes:

$$\text{BrierScore} = \frac{1}{n} \sum_{i=1}^n (\hat{p}_i - y_i)^2. \quad (8)$$

Lower values of either metric indicate better-calibrated predictions.

By selecting the model that has the minimum ECE, we obtain calibrated softmax values $g(y_i)$. Furthermore, to ensure that samples are spread evenly across bins to support our statistical guarantees, we perform *adaptive binning* as defined below to construct a validation dataset Z_{val} , on which we obtain our guarantees.

Definition 9 (Adaptive binning) Given a dataset Z , split Z into Q bins $\{B_j\}_{j=1}^Q$ by a constant count of samples, $\lfloor |Z|/Q \rfloor$ each. The resulting $\{B_j\}_{j=1}^Q$ is a binned dataset. From each bin B_j , we draw N i.i.d. samples with replacement M times to get $\{B_{j1}, \dots, B_{jM}\}$. For

each resampled bin B_{ji} , we calculate

$$\begin{aligned} g_{ji} &= \frac{1}{|B_{ji}|} \sum_{y \in B_{ji}} g(y), \\ p_{ji} &= \frac{1}{|B_{ji}|} \sum_{y \in B_{ji}} \mathbf{1}\{\text{prediction is safe}\}, \\ \delta_{ji} &:= |g_{ji} - p_{ji}|. \end{aligned}$$

Given a bin number j , our goal is to build prediction intervals $[0, c_j]$ that contain the calibration error of the next (unknown) average confidence g_{j^*} that falls into bin B_j with chance at least $1 - \alpha$:

$$P(|g_{j^*} - p_j| \leq c_j) \geq 1 - \alpha \quad \text{for } j = 1, \dots, Q, \quad (9)$$

where α is the miscoverage level (a hyperparameter).

That is, we aim to find a statistical upper bound c_j on the error of our chance predictor in each bin. After we obtain a chance prediction g_{j^*} , it will be turned into an *uncertainty-aware interval*:¹

$$[g_{j^*} - c_j, g_{j^*} + c_j],$$

which contains the true probability of safety in $1 - \alpha$ cases. Notice that this guarantee is relative to the binned dataset fixed in Definition 9.

To provide this guarantee, we apply conformal prediction in Algorithm 1 [115]. Intuitively, we rank the safety chance errors in resampled bins and obtain a statistical upper bound on this error for each bin. Similarly to existing works relying on conformal prediction, this algorithm guarantees equation (9) [25, 116]. Recall that each calibration example $(\mathbf{y}_i, \varphi(x_{i+k}))$ is drawn from an independent trajectory, so the calibration set satisfies the i.i.d. assumption required by conformal prediction.

Theorem 1 (Conformal Bounds on Confidence Scores (adaptation of Theorem 2.1 in Lei et al. 2018[115])) *Given a dataset bin $B = \{b_k\}_{k=1}^K$ of i.i.d. observation-state pairs $b_k = (y_k, x_k)$, we obtain a collection of datasets $\{B_j\}_{j=1}^M$ by drawing M datasets of N i.i.d. samples from B , leading to datasets B_j to be drawn i.i.d. from a dataset distribution \mathcal{D} . Then for another, unseen dataset $B_{M+1} \sim \mathcal{D}$, safety chance predictor g , and miscoverage level α , calculating*

$$c = \text{ConCali}(B, g, \alpha)$$

leads to prediction intervals with guaranteed containment:

$$P_{\mathcal{D}}(|q(B_{M+1}) - p(B_{M+1})| \leq c) \geq 1 - \alpha,$$

where $q(B_{M+1})$ is the mean safety chance prediction in B_{M+1} :

$$q(B_{M+1}) \leftarrow \frac{1}{N} \sum_{l=1}^N g(y_l), \quad \text{for each } y_l \in B_{M+1}.$$

¹This is an interval on confidence, rather than a confidence interval.

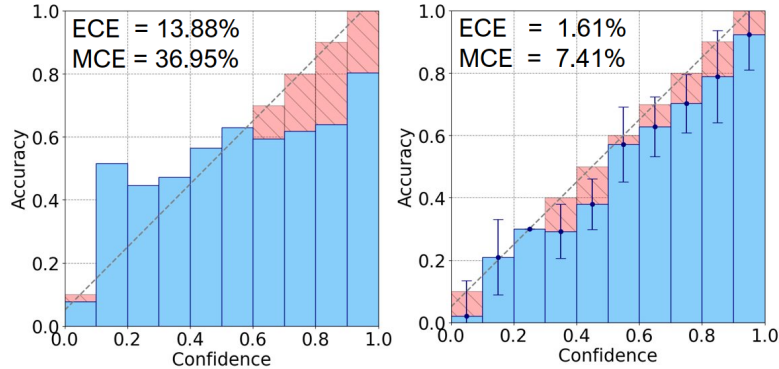


Fig. 4 Calibration of a monolithic CNN predictor for the racing car with horizon $k = 100$. Left: uncalibrated, right: calibrated via isotonic regression and conformal bounds for $\alpha = 0.05$.

and $p(B_{M+1})$ is the mean true safety chance in B_{M+1} :

$$p(B_{M+1}) \leftarrow \frac{1}{N} \sum_{i=1}^N \phi(x_i), \quad \text{for each } \phi(x_i) \in B_{M+1},$$

where $\phi(x)$ is the safety of x .

Proof The proof follows the same structure as Theorem 2.1 in Lei et al. 2018, with the modification that non-conformity scores are computed on average safety probabilities within bins [115]. Given that resampled bins B_j are drawn i.i.d. from \mathcal{D} , the exchangeability assumption required by conformal prediction still holds. Therefore, ranking the absolute deviations δ_j yields the $(1 - \alpha)$ coverage guarantee in (9). \square

5 Experimental Evaluation

Benchmark Systems

The racing car and cart pole from the OpenAI Gym and the realistic donkey car are selected as our study cases [117]. These environments are more suitable than pre-collected robotic datasets, such as the Waymo Open Dataset, for two reasons. First, to study safety prediction, we require a large dataset of safety violations, which is rarely found in real-world data. Second, the simulated dynamical systems are convenient for collecting an unbounded amount of data with direct access to the images and the ground truth for experimental evaluation (e.g., the car’s position).

We defined the racing car’s safety as being located within the track surface. The cart pole’s safety is defined by the angles in the safe range of $[-6, 6]$ degrees, whereas the whole activity range of the cart pole is $[-48, 48]$ degrees. For the donkey car driving on a two-lane track, staying in the right lane is safe, whereas crossing over the lane boundary is unsafe.

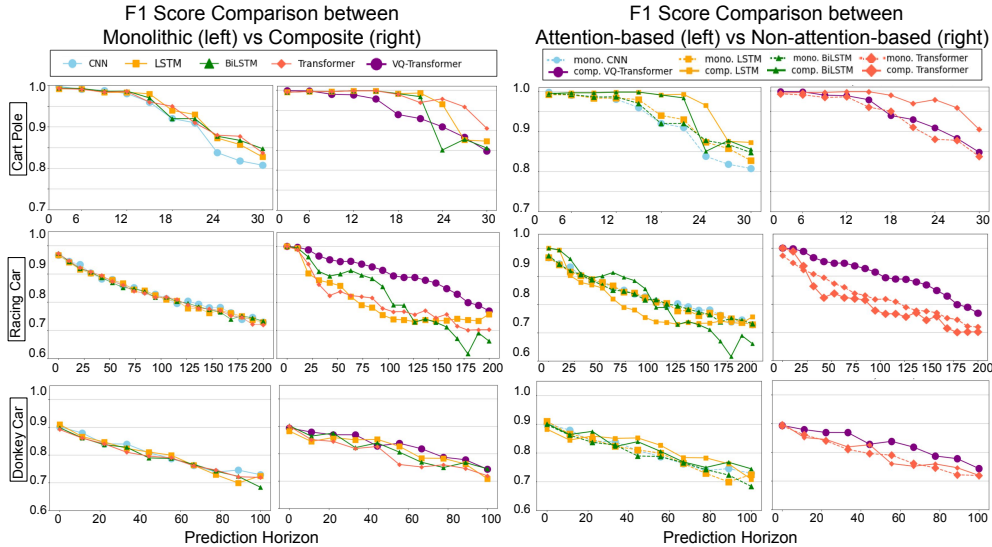


Fig. 5 F1 score performance of safety label predictors over varied horizons. Upper to Lower: (1) cart pole; (2) car racing; (3) donkey car. Left pairs show the comparison between monolithic (mon.) models and composite (comp.) models, while right pairs show the comparison between attention-based models and non-attention-based models.

Performance Metrics

We use the *F1 score* as our main metric for evaluating the accuracy of safety label predictors, as it balances the precision and recall:

$$F1 = 2 \times \frac{\text{Precision} \times \text{Recall}}{\text{Precision} + \text{Recall}} = 2 \times \frac{TP}{TP + \frac{FP+FN}{2}}.$$

False positives are also a major concern in safety prediction (actually unsafe situations predicted as safe), so we also evaluate the *False Positive Rate* (FPR):

$$\text{FPR} = \frac{FP}{FP + TN}.$$

To evaluate our chance predictors, we compute the *Expected Calibration Error* (ECE, intuitively a weighted average difference between the predicted and true probabilities) and the *Brier Score* (mean squared error between predicted probabilities and actual binary outcomes) [12, 13, 114].

5.1 Experimental Setup

Hardware

The computationally heavy training was performed on a single NVIDIA A100 GPU, and other light tasks like data collection and conformal calibration were done on a

CPU workstation with a 12th Gen Intel Core i9-12900H CPU and 64GB RAM in Ubuntu 22.04.

Datasets

Deep Q-networks (DQN) were used to implement image-based controllers both for the racing car and the cart pole. For the racing car, we collected 240K samples for training and 60K for calibration/validation/testing each. For the cart pole, we collected 90K samples for each of the four datasets. All images were processed with normalization, which facilitated stable model training and improved generalization across different environments.

Each case study’s data is randomly partitioned into four datasets. All the training tasks for the predictors are performed on the training dataset \mathbf{Z}_{tr} . The calibration dataset \mathbf{Z}_{cal} is to tune predictor hyperparameters and fit the calibrators. The validation dataset \mathbf{Z}_{val} is used to produce conformal guarantees, and finally, the test dataset \mathbf{Z}_{te} is used to compute the performance metrics like F1, FPR, ECE, and Brier scores.

5.1.1 Training details

Pytorch 1.13.1 with the Adam optimizer was used for training. The maximum training epoch is 500 for VAEs and 100 for predictors. The safety loss in the Equation. 2 uses $\lambda_1 = 1$ and $\lambda_2 = 4096$, which equals the total pixel count in our images. The miscoverage level is $\alpha = 0.05$. We used the Adam optimizer (initial learning rate 10^{-3} , reduced by a factor of 0.1 with a patience of 5 epochs) and early stopping with a patience of 15 epochs. The maximum training epochs were 500 for VAEs and 100 for predictors. Batch sizes were 128 for classifiers, 64 for latent predictors, and 16 for image predictors. The CNN-based evaluator and single-image predictor used two convolutional layers (kernels 3 and 5) with max-pooling, followed by three linear layers and a softmax. The VAE encoder had four convolutional layers and two linear layers (latent size 32), and the decoder mirrored this with transposed convolutions. Sequence models used one LSTM layer and one linear layer, with monolithic predictors outputting 2 classes and composite latent forecasters outputting 32-dimensional vectors. For each test sample, multiple augmented views are generated using seven types of transformations: autocontrast, equalize, rotation, solarization, shear, translation, and posterization in our UDA. These augmentations alter low-level visual attributes while preserving the semantic content of the original image. The model’s predictions over these views are aggregated, and the network parameters are adapted to improve stability and robustness against domain variations for our evaluator. We released our code at <https://github.com/Trustworthy-Engineered-Autonomy-Lab/hsai-predictor>.

5.2 Comparative Results

Below, we present comparisons and ablations along the six key dimensions of the proposed family of predictors and also discuss our conformal calibration’s performance. In the figures and tables, “mon” and “comp” stand for monolithic and composite, respectively.

Table 1 F1 Score and FPR.

Model	Racing Car			Cart Pole			Donkey Car		
	k=60	k=120	k=180	k=10	k=20	k=30	k=30	k=60	k=90
F1 score									
mono. CNN	88.04	79.51	73.83	99.65	94.45	95.21	88.99	83.73	77.18
mono. LSTM	87.89	80.48	74.95	98.29	93.97	85.72	84.69	79.92	69.89
mono. BiLSTM	86.88	80.24	75.09	98.59	91.35	86.76	83.69	78.72	72.27
mono. Transformer	87.34	80.89	74.55	98.38	94.45	87.21	88.99	77.83	73.25
comp. LSTM	85.99	73.67	73.60	99.65	99.11	87.50	85.87	82.66	76.19
comp. BiLSTM	90.17	78.93	61.54	99.65	98.37	87.02	87.49	80.55	76.73
comp. Transformer	83.83	76.62	70.18	99.47	98.93	95.21	84.46	76.03	74.59
comp. VQ-Transformer	94.55	89.35	79.03	98.65	93.83	88.21	88.18	83.73	77.18
FPR									
mono. CNN	27.25	39.48	54.11	8.41	28.43	34.39	26.35	37.16	42.83
mono. LSTM	26.57	35.30	44.56	5.31	24.12	36.44	24.89	35.16	38.66
mono. BiLSTM	26.69	36.35	45.34	10.36	22.27	35.93	27.47	33.63	47.54
mono. Transformer	25.48	36.81	42.80	13.86	34.08	37.29	25.76	31.29	40.33
comp. LSTM	16.75	23.98	35.41	10.38	19.68	39.45	32.56	30.46	36.71
comp. BiLSTM	28.57	30.71	34.29	3.09	16.92	46.33	28.87	27.23	40.37
comp. Transformer	17.13	26.56	35.71	14.51	30.91	31.34	41.10	30.36	47.90
comp. VQ-Transformer	18.18	27.01	35.72	3.56	24.94	28.28	32.12	34.73	41.92

Composite predictors outperform monolithic ones

Monolithic predictors use their full learning capacity to predict safety but do not learn the underlying dynamics. Therefore, our initial hypothesis was that they would do well on short horizons — but lose to composite predictors on longer horizons. The results support this hypothesis, as illustrated in Figure 5: the performance of monolithic predictors degrades faster as the horizon grows. Moreover, composite predictors offered a better FPR as shown in Table 1 for the donkey cars, which may be desirable in safety-critical systems. We contend that the inferior performance of monolithic predictors arises from the inherent difficulty of learning coherent, long-term latent dynamics — a challenge that remains largely unresolved. By contrast, composite predictors achieve superior results by explicitly decomposing the safety-prediction problem into three stages: (1) learning a suitable latent representation; (2) forecasting future states, and (3) evaluating those states’ safety. This architectural separation imposes a clear inductive bias: the model is first guided to generate plausible trajectories and then to judge their safety, rather than expecting a single network to discover both the underlying dynamics and the safety criterion simultaneously. As a result, each subtask becomes substantially more tractable, leading to higher overall performance.

Attention significantly improves composite predictor performance

Incorporating attention blocks via transformers into the composite predictor architecture yielded consistent improvements in both FPR and F1 scores across all forecasting horizons as shown in Table 1. This suggests that leveraging both past and future context enhances the model’s ability to produce temporally coherent and accurate

Table 2 ECE and Brier Score before (gray rows) and after (white rows) calibration.

Model	Racing Car			Cart Pole			Donkey Car		
	k=60	k=120	k=180	k=10	k=20	k=30	k=30	k=60	k=90
ECE									
mono. CNN	0.0715	0.1349	0.1390	0.1348	0.4031	0.7393	0.0664	0.1807	0.2798
mono. CNN	0.0079	0.0094	0.0090	0.0031	0.0030	0.0057	0.0292	0.0614	0.0745
mono. LSTM	0.1197	0.1868	0.1675	0.0014	0.0096	0.2121	0.1447	0.2102	0.3336
mono. LSTM	0.0054	0.0100	0.0119	0.0007	0.0038	0.0176	0.0958	0.1971	0.2075
mono. BiLSTM	0.1558	0.2506	0.1905	0.0038	0.0018	0.1483	0.1702	0.2646	0.2705
mono. BiLSTM	0.0133	0.0149	0.0467	0.0029	0.0006	0.0127	0.1286	0.1521	0.2354
mono. Transformer	0.1019	0.1121	0.3011	0.7341	0.4201	0.6722	0.0897	0.1751	0.2689
mono. Transformer	0.0164	0.0095	0.0194	0.0008	0.0023	0.0164	0.0667	0.0704	0.0875
comp. LSTM	0.0052	0.0012	0.0039	0.1069	0.4659	0.5264	0.1112	0.1304	0.2425
comp. LSTM	0.0002	0.0002	0.0007	0.0045	0.0088	0.0119	0.0405	0.0864	0.0320
comp. BiLSTM	0.2165	0.0725	0.1646	0.0914	0.3388	0.4635	0.1171	0.1727	0.2108
comp. BiLSTM	0.0093	0.0159	0.0215	0.0834	0.1086	0.1419	0.0249	0.0809	0.1280
comp. Transformer	0.1803	0.3511	0.5474	0.1437	0.0281	0.0826	0.0851	0.1215	0.2034
comp. Transformer	0.0074	0.0005	0.0143	0.0051	0.0255	0.0107	0.0769	0.0084	0.0589
comp. VQ-Transformer	0.0144	0.0026	0.0515	0.0100	0.1426	0.2589	0.0661	0.1229	0.2209
comp. VQ-Transformer	0.0008	0.0032	0.0002	0.0026	0.0082	0.0111	0.0038	0.0739	0.1455
Brier Score									
mono. CNN	0.2269	0.2708	0.2400	0.0022	0.0405	0.1895	0.1298	0.2452	0.2680
mono. CNN	0.1306	0.1067	0.1269	0.0018	0.0136	0.0720	0.1075	0.1287	0.2162
mono. LSTM	0.1965	0.3317	0.3079	0.0017	0.0275	0.1521	0.1547	0.2486	0.2834
mono. LSTM	0.0020	0.0993	0.1804	0.0011	0.0180	0.1365	0.0095	0.0527	0.1644
mono. BiLSTM	0.1083	0.4916	0.2017	0.2822	0.5659	0.3453	0.0399	0.1038	0.1902
mono. BiLSTM	0.0796	0.2248	0.1619	0.0039	0.0184	0.1518	0.0042	0.0186	0.0728
mono. Transformer	0.0126	0.2556	0.1777	0.4970	0.9131	0.6400	0.0734	0.0971	0.1611
mono. Transformer	0.0235	0.0523	0.0939	0.0197	0.0159	0.0382	0.0697	0.0797	0.1223
comp. LSTM	0.1938	0.2663	0.3749	0.1975	0.1281	0.3551	0.1197	0.1214	0.1568
comp. LSTM	0.1666	0.2318	0.2635	0.0519	0.0533	0.1045	0.0866	0.0957	0.1383
comp. BiLSTM	0.2742	0.3393	0.3688	0.0915	0.2025	0.3337	0.0986	0.1117	0.1574
comp. BiLSTM	0.1343	0.2026	0.1937	0.0280	0.0211	0.1255	0.0836	0.0932	0.1501
comp. Transformer	0.1152	0.1491	0.2169	0.119	0.2474	0.2782	0.0648	0.0813	0.0903
comp. Transformer	0.0645	0.0981	0.1150	0.0638	0.0812	0.0987	0.0222	0.0774	0.0786
comp. VQ-Transformer	0.0674	0.2380	0.2587	0.2035	0.2584	0.2411	0.0792	0.0887	0.0975
comp. VQ-Transformer	0.0600	0.0559	0.0521	0.0554	0.0617	0.0774	0.0544	0.0616	0.0951

Table 3 F1 scores of evaluators on different datasets (in %).

Case Study	Evaluator Type	Normal	OOD	Mix
Racing Car	Image Evaluator	99.56	63.94	78.23
	Latent Evaluator	98.79	65.73	80.27
	UDA Image Evaluator	97.13	81.65	91.34
Cart Pole	Image Evaluator	99.66	67.21	91.05
	Latent Evaluator	99.67	69.14	89.33
	UDA Image Evaluator	99.06	76.52	96.62
Donkey Car	Image Evaluator	96.20	93.03	94.43
	Latent Evaluator	97.19	92.21	94.70
	UDA Image Evaluator	96.05	94.14	95.97

predictions. Additionally, we observed a substantial decrease in ECE as indicated in Table 2, indicating that the VQ-transformers not only perform better but also make significantly more calibrated predictions.

Table 4 FPR of evaluators on different datasets (in %).

Case Study	Evaluator Type	Normal	OOD	Mix
Racing Car	Image Evaluator	0.42	52.78	23.53
	Latent Evaluator	2.15	30.82	19.62
	UDA Image Evaluator	0.62	7.07	4.37
Cart Pole	Image Evaluator	0.53	21.51	9.88
	Latent Evaluator	0.61	18.34	7.69
	UDA Image Evaluator	1.34	16.72	10.03
Donkey Car	Image Evaluator	2.69	18.25	6.05
	Latent Evaluator	3.05	11.97	5.32
	UDA Image Evaluator	3.21	9.15	5.42

Latent evaluators outperform image-based ones

Latent evaluators outperform image-based ones both in F1 and FPR, as shown in the Tables 3 and 4. This is primarily because the VAE’s reconstruction objective encourages the latent space to capture fine-grained image details, while the prior imposes additional structure that facilitates classification. Moreover, KL regularization promotes smoothness of the latent manifold and can implicitly disentangle task-relevant features. Additionally, the latent representation filters out pixel-level noise and, by mapping sequential observations into a compact and structured manifold, preserves the temporal relationships between states. This smoothness in latent trajectories makes it easier for the evaluator to capture long-term safety-relevant dynamics and avoid being misled by transient visual variations.

UDA evaluator improves robustness under distribution shift

We evaluate the effectiveness of unsupervised domain adaptation in enhancing the evaluator’s robustness to distribution shift. In addition to the normal images, we test on two special test subsets: *OOD*, which consists of 500 images sampled from predictions with manual labels that exhibit strong distribution shift, and *Mix*, which randomly selects 500 predictions containing both in-distribution and OOD examples, with proportions varying by case study. As shown in Tables 3 and 4, across all case studies, UDA-based image evaluators consistently outperform both standard image and latent evaluators on the OOD and Mix subsets, without losing almost any performance on the normal data. These results demonstrate that UDA is a promising technique to generalize safety evaluators to challenging out-of-distribution scenarios.

Calibration improves safety-chance predictor reliability.

The reliability diagram in Figure 4 exemplifies a common situation among uncalibrated chance predictors: underconfident for the rejected class (below 0.5), overconfident for the chosen class (above 0.5). The aggregate calibrated results for different architectures and prediction horizons are shown in Table 2. We can see that our calibration consistently reduces the overconfidence and leads to a lower ECE, even for long prediction horizons. The most effective calibrators were the isotonic regression for the racing car and ENIR for the cart pole and donkey car. This leads us to conclude that

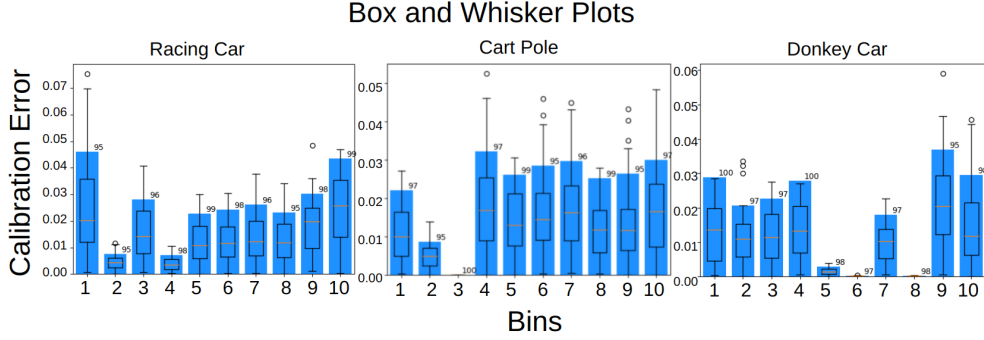


Fig. 6 Our conformal bounds (in blue) for calibration error of the monolithic predictor (left to right: racing car, cart pole, and donkey car) with horizon $k = 18$ for $\alpha = 0.05$ contain more than 95% of the true calibration errors (box and whisker plots).

safety-chance prediction is a more suitable problem formulation for highly uncertain image-controlled robots rather than safety-label prediction.

Conformal calibration coverage is reliable

Supporting our theoretical claims, the predicted intervals for calibration errors contained the true error values from the test data (Figure 6). The coverage for the racing car is $96.24\% \pm 4.75\%$, the cart pole is $96.09\% \pm 5.71\%$, and the donkey car is $98.52\% \pm 3.76\%$. Our average error bound is 0.0924 ± 0.0438 for the racing car, 0.0409 ± 0.0200 for the cartpole, and 0.0628 ± 0.0296 for the donkey car. Therefore, our calibration intervals, constructed as predicted chance \pm its bin’s calibration bound, can be used reliably and informatively in online robotic tasks like prediction, planning, and adaptation.

6 Discussion and Conclusion

Limitations

Our predictor family’s scope is limited to systems where safety can be inferred from raw sensor data. This assumption holds in domains like autonomous driving, where an imminent collision, lane departure, or off-track event can be visually detected. Relatedly, the safety specifications considered in this work are restricted to simple state-based binary predicates ($\varphi : \mathcal{X} \rightarrow \{0, 1\}$) and do not capture temporal requirements. In contrast, there exist systems where safety depends on unobservable internal states or variables that are not visually apparent. For example, for an aircraft whose structural integrity depends on internal component stresses, raw visual or range data would be insufficient to assess safety.

Obtaining labeled safety data is associated with notable costs, especially for negative safety samples in physical systems. Our approach is limited to systems where it is possible to generate a large volume of labeled data to effectively train the predictors. For instance, our donkey car case study required labeling over 10,000 images,

which took approximately 5-10 hours of human effort, including iterative refinement. While this labeling burden is non-trivial, it is feasible for many robotics applications where safety-critical scenarios can be systematically collected. Furthermore, this burden can be substantially alleviated through automated and semi-automated labeling techniques. Recent frameworks for active learning, weak supervision, and programmatic labeling have demonstrated significant reductions in manual annotation effort for similar vision-based tasks [118–120].

Some prediction approaches have performed poorly, like monolithic *flexible-horizon* predictors, which output the time to the first expected safety violation. Their prediction space appeared too complex and insufficiently regularized, leading to poor learning and performance. Also, existing test-time adaptation methods operate at the image level, which is potentially inefficient. Exploring adaptation in latent representation could further improve the performance of the latent evaluator under distribution shift. Thus, learning strong safety-informed representations for autonomy remains an open problem. With the rise of large language models, meaning representations in multimodal autoregressive models may provide more possibilities to explore the surrogate dynamics of autonomy systems [112].

Future work

Interesting future directions include adding physical constraints to latent states similar to Neural ODEs, using a generative model to obtain surrogate unsafe samples from a more realistic environment, and applying vision-language and vision-language-action models to automatically label the safety of generative predictions [121]. Another opportunity is to mitigate the labeling burden via transfer learning from simulation and generative models. Furthermore, our framework can be extended to support safety specifications in linear temporal logic (LTL), enabling safety predictions that reason over sequences of events and long-horizon behavioral constraints [122].

Declarations

Acknowledgments

First, the authors would like to thank Cade McGlothlin and Rohith Nama Reddy for experimenting with prediction architectures. Second, they would like to thank Srikruth Puram, Shaurya Wahal, and Pham “Tony” Hung for their work on various simulators. Finally, the authors also thank Dong-You “Sam” Jhong, Ao Wang, Chenxi Zhou, and Cesar Valentin for setting up Donkey Cars.

Funding

The authors disclose receipt of the following financial support for the research, authorship, and publication of this article. This work was supported in part by the NSF Grant CNS 2513076. Any opinions, findings, or conclusions expressed in this material are those of the authors and do not necessarily reflect the views of the National Science Foundation (NSF) or the U.S. Government.

References

- [1] Sorin Grigorescu, Bogdan Trasnea, Teodora Cocias, and Gheorghe Macesanu. A survey of deep learning techniques for autonomous driving. *Journal of Field Robotics*, 37(3):362–386, 2020. doi: 10.1002/rob.21918.
- [2] Egemen Yurtsever, Julien Lambert, Alejandro Carballo, and Kazunori Takeda. A survey of autonomous driving: Common practices and emerging technologies. *IEEE Access*, 8:58443–58469, 2020. doi: 10.1109/ACCESS.2020.2973615.
- [3] Xinyu Liu, Hu Zhang, and Wei Li. Multimodal sensor fusion and deep learning for autonomous driving: A review. *IEEE Transactions on Intelligent Transportation Systems*, 2024. doi: 10.1109/TITS.2024.3376543. Early Access.
- [4] Mariusz Bojarski, Davide Del Testa, Daniel Dworakowski, Bernhard Firner, Beat Flepp, Praseon Goyal, Lawrence D. Jackel, Mathew Monfort, Urs Muller, Jiakai Zhang, Xin Zhang, Jake Zhao, and Karol Zieba. End to End Learning for Self-Driving Cars, April 2016. URL <http://arxiv.org/abs/1604.07316>. arXiv:1604.07316 [cs].
- [5] Felipe Codevilla, Matthias Müller, Alexey Dosovitskiy, Antonio Lopez, and Vladlen Koltun. End-to-end driving via conditional imitation learning. In *Proceedings of the IEEE International Conference on Robotics and Automation (ICRA)*, pages 4693–4700, 2018. doi: 10.1109/ICRA.2018.8460487.
- [6] Ravi Kiran, Ibrahim Sobh, Vincent Talpaert, Patrick Mannion, Ahmad Al Salhab, Senthil Yogamani, and Patrick Pérez. Deep reinforcement learning for autonomous driving: A survey. *IEEE Transactions on Intelligent Transportation Systems*, 23(6):4909–4926, 2022. doi: 10.1109/TITS.2021.3134702.
- [7] Anton Kuznetsov, Balint Gyevnar, Cheng Wang, Steven Peters, and Stefano V. Albrecht. Explainable AI for Safe and Trustworthy Autonomous Driving: A Systematic Review, July 2024. URL <http://arxiv.org/abs/2402.10086>. arXiv:2402.10086.
- [8] Simon Hecker, Dengxin Dai, and Luc Van Gool. Failure prediction for autonomous driving. *IEEE Intelligent Vehicles Symposium*, 2018.
- [9] Angelos Filos, Panagiotis Tigas, Rowan McAllister, Nicholas Rhinehart, Sergey Levine, and Yarin Gal. Can autonomous vehicles identify, recover from, and adapt to distribution shifts? *International Conference on Machine Learning*, 2020.
- [10] Praveena Penmetsa, Pezhman Sheinidashtegol, Aibek Musaev, Emmanuel Kofi Adanu, and Matthew Hudnall. Effects of the autonomous vehicle crashes on public perception of the technology. *IATSS Research*, 45(4):485–492, 2021. doi: 10.1016/j.iatssr.2021.04.003.

- [11] Tesla. Autonomous vehicle trajectory prediction using vision-only deep learning. Tesla AI Day 2025, 2025. URL <https://www.tesla.com/ai>.
- [12] Chuan Guo, Geoff Pleiss, Yu Sun, and Kilian Q. Weinberger. On calibration of modern neural networks. In *Proceedings of the 34th International Conference on Machine Learning - Volume 70, ICML'17*, pages 1321–1330, Sydney, NSW, Australia, August 2017. JMLR.org.
- [13] Matthias Minderer, Josip Djolonga, Rob Romijnders, Frances Hubis, Xiaohua Zhai, Neil Houlsby, Dustin Tran, and Mario Lucic. Revisiting the Calibration of Modern Neural Networks. In *Advances in Neural Information Processing Systems*, volume 34, pages 15682–15694. Curran Associates, Inc., 2021.
- [14] Björn Lütjens, Michael Everett, and Jonathan P. How. Safe reinforcement learning with model uncertainty estimates. *arXiv preprint arXiv:1810.08700*, 2018.
- [15] Di Feng, Lars Rosenbaum, Claudius Glaeser, Fabian Timm, and Klaus Dietmayer. Can we trust you? on calibration of a probabilistic object detector for autonomous driving. *arXiv preprint arXiv:1909.12358*, 2019.
- [16] Aniketh Ramesh, Rustam Stolkin, and Manolis Chiou. Robot vitals and robot health: Towards systematically quantifying runtime performance degradation in robots under adverse conditions. *IEEE Robotics and Automation Letters*, 7(4): 10729–10736, 2022. doi: 10.1109/LRA.2022.3192612.
- [17] Alvika Gautam, Tim Whiting, Xuan Cao, Michael A. Goodrich, and Jacob W. Crandall. A method for designing autonomous robots that know their limits. In *Proceedings of the IEEE International Conference on Robotics and Automation (ICRA)*, pages 121–127, 2022. doi: 10.1109/ICRA46639.2022.9812030.
- [18] Ivan Ruchkin, Matthew Cleaveland, Radoslav Ivanov, Pengyuan Lu, Taylor Carpenter, Oleg Sokolsky, and Insup Lee. Confidence Composition for Monitors of Verification Assumptions. In *ACM/IEEE 13th Intl. Conf. on Cyber-Physical Systems (ICCPS)*, pages 1–12, May 2022. doi: 10.1109/ICCPS54341.2022.00007.
- [19] Nicholas Conlon, Nisar Ahmed, and Daniel Szafir. Event-triggered robot self-assessment to aid in autonomy adjustment. *Frontiers in Robotics and AI*, 10, 2024. doi: 10.3389/frobt.2023.1294533.
- [20] Michael Everett, Golnaz Habibi, and Jonathan P. How. Efficient reachability analysis of closed-loop systems with neural network controllers. In *IEEE International Conference on Robotics and Automation (ICRA)*, 2021. doi: 10.1109/ICRA48506.2021.9561348.
- [21] Saeid Toufighi and Mark Girolami. Decision boundary learning for safe vision-based navigation via hamilton-jacobi reachability. In *Proceedings of the*

- [22] Sayan Mitra, Corina Păsăreanu, Pavithra Prabhakar, Sanjit A. Seshia, Ravi Mangal, Yangge Li, Christopher Watson, Divya Gopinath, and Huafeng Yu. Formal Verification Techniques for Vision-Based Autonomous Systems – A Survey. In Nils Jansen, Sebastian Junges, Benjamin Lucien Kaminski, Christoph Matheja, Thomas Noll, Tim Quatmann, Mariëlle Stoelinga, and Matthias Volk, editors, *Principles of Verification: Cycling the Probabilistic Landscape : Essays Dedicated to Joost-Pieter Katoen on the Occasion of His 60th Birthday, Part III*, pages 89–108. Springer Nature Switzerland, Cham, 2025. ISBN 978-3-031-75778-5. doi: 10.1007/978-3-031-75778-5_5. URL https://doi.org/10.1007/978-3-031-75778-5_5.
- [23] Alexandre Donze and Oded Maler. Robust Satisfaction of Temporal Logic over Real-Valued Signals. In Krishnendu Chatterjee and Thomas A. Henzinger, editors, *Formal Modeling and Analysis of Timed Systems*, Lecture Notes in Computer Science, pages 92–106. Springer Berlin Heidelberg, 2010. ISBN 978-3-642-15297-9.
- [24] Manuel Müller, Golsa Ghasemi, Nasser Jazdi, and Michael Weyrich. Situational risk assessment design for autonomous mobile robots. *Procedia CIRP*, 109:412–417, 2022.
- [25] Lars Lindemann, Xin Qin, Jyotirmoy V. Deshmukh, and George J. Pappas. Conformal Prediction for STL Runtime Verification. In *Proc. of ICCPS'23*, San Antonio, TX, March 2023. arXiv. doi: 10.48550/arXiv.2211.01539. URL <http://arxiv.org/abs/2211.01539>. arXiv:2211.01539 [cs, eess].
- [26] Xiaosong Jia, Penghao Wu, Li Chen, Yu Liu, Hongyang Li, and Junchi Yan. Hdgt: Heterogeneous driving graph transformer for multi-agent trajectory prediction via scene encoding. arXiv preprint arXiv:2205.09753, 2022. URL <https://arxiv.org/abs/2205.09753>.
- [27] Mingkun Wang, Xiaoguang Ren, Ruochun Jin, Minglong Li, Xiaochuan Zhang, Changqian Yu, Mingxu Wang, and Wenjing Yang. FutureNet-lof: Joint trajectory prediction and lane occupancy field prediction with future context encoding. arXiv preprint arXiv:2406.14422, 2024. URL <https://arxiv.org/abs/2406.14422>.
- [28] Zhigang Sun, Zixu Wang, Lavdim Halilaj, and Juergen Luetttin. Semanticformer: Holistic and semantic traffic scene representation for trajectory prediction using knowledge graphs. *IEEE Robotics and Automation Letters*, 2024. URL <https://arxiv.org/abs/2404.19379>. Preprint: arXiv:2404.19379.
- [29] Jingkan Yang, Kaiyang Zhou, Yixuan Li, and Ziwei Liu. Generalized out-of-distribution detection: A survey. *International Journal of Computer Vision*, 132(12):5635–5662, 2024.

- [30] Zhenjiang Mao, Carson Sobolewski, and Ivan Ruchkin. How safe am i given what i see? calibrated prediction of safety chances for image-controlled autonomy. In *6th Annual Learning for Dynamics & Control Conference*, pages 1370–1387. PMLR, 2024.
- [31] Ari Viitala, Rinu Boney, Yi Zhao, Alexander Ilin, and Juho Kahala. Learning to Drive (L2D) as a Low-Cost Benchmark for Real-World Reinforcement Learning. In *20th International Conference on Advanced Robotics, ICAR*, pages 275–281. IEEE, 2021. doi: 10.1109/ICAR53236.2021.9659342. URL <https://research.aalto.fi/en/publications/learning-to-drive-l2d-as-a-low-cost-benchmark-for-real-world-rein>.
- [32] Ari Viitala. *Scale Model Autonomous Driving Benchmark for Deep Reinforcement Learning Algorithms*. PhD thesis, August 2021. URL <https://aaltodoc.aalto.fi/handle/123456789/109412>.
- [33] Samer Ammoun and Fawzi Nashashibi. Real time trajectory prediction for collision risk estimation between vehicles. In *2009 IEEE 5th International Conference on Intelligent Computer Communication and Processing*, pages 417–422, 2009. doi: 10.1109/ICCP.2009.5284727.
- [34] Stéphanie Lefèvre, Dizan Vasquez, and Christian Laugier. A survey on motion prediction and risk assessment for intelligent vehicles. *ROBOMECH Journal*, 1(1):1, July 2014. ISSN 2197-4225. doi: 10.1186/s40648-014-0001-z. URL <https://doi.org/10.1186/s40648-014-0001-z>.
- [35] Anjian Li, Liting Sun, Wei Zhan, Masayoshi Tomizuka, and Mo Chen. Prediction-Based Reachability for Collision Avoidance in Autonomous Driving. In *2021 IEEE International Conference on Robotics and Automation (ICRA)*, pages 7908–7914, May 2021. doi: 10.1109/ICRA48506.2021.9560790. ISSN: 2577-087X.
- [36] Kensuke Nakamura and Somil Bansal. Online update of safety assurances using confidence-based predictions, 2023.
- [37] Yanjun Huang, Jiatong Du, Ziru Yang, Zewei Zhou, Lin Zhang, and Hong Chen. A Survey on Trajectory-Prediction Methods for Autonomous Driving. *IEEE Transactions on Intelligent Vehicles*, 7(3):652–674, September 2022. ISSN 2379-8904. doi: 10.1109/TIV.2022.3167103. Conference Name: IEEE Transactions on Intelligent Vehicles.
- [38] Tim Salzmann, Boris Ivanovic, Punarjay Chakravarty, and Marco Pavone. Trajectron++: Dynamically-Feasible Trajectory Forecasting with Heterogeneous Data. In *Computer Vision – ECCV 2020*, Lecture Notes in Computer Science, pages 683–700, Cham, 2020. Springer International Publishing. ISBN 978-3-030-58523-5. doi: 10.1007/978-3-030-58523-5_40.

- [39] Kihyuk Sohn, Honglak Lee, and Xinchen Yan. Learning structured output representation using deep conditional generative models. In C. Cortes, N. Lawrence, D. Lee, M. Sugiyama, and R. Garnett, editors, *Advances in Neural Information Processing Systems*, volume 28. Curran Associates, Inc., 2015. URL https://proceedings.neurips.cc/paper_files/paper/2015/file/8d55a249e6baa5c06772297520da2051-Paper.pdf.
- [40] Anish Muthali, Haotian Shen, Sampada Deglurkar, Michael H. Lim, Rebecca Roelofs, Aleksandra Faust, and Claire Tomlin. Multi-Agent Reachability Calibration with Conformal Prediction, April 2023. URL <http://arxiv.org/abs/2304.00432>. arXiv:2304.00432 [cs, eess].
- [41] Anushri Dixit, Lars Lindemann, Skylar X Wei, Matthew Cleaveland, George J Pappas, and Joel W Burdick. Adaptive conformal prediction for motion planning among dynamic agents. In *Learning for Dynamics and Control Conference*, pages 300–314. PMLR, 2023.
- [42] Juanwu Lu, Wei Zhan, Masayoshi Tomizuka, and Yeping Hu. Towards generalizable and interpretable motion prediction: A deep variational bayes approach. In *International Conference on Artificial Intelligence and Statistics*, pages 4717–4725. PMLR, 2024.
- [43] Masha Itkina and Mykel Kochenderfer. Interpretable self-aware neural networks for robust trajectory prediction. In *Conference on Robot Learning*, pages 606–617. PMLR, 2023.
- [44] Jordan Peper, Zhenjiang Mao, Yuang Geng, Siyuan Pan, and Ivan Ruchkin. Four principles for physically interpretable world models. *arXiv preprint arXiv:2503.02143*, 2025.
- [45] Zhenjiang Mao and Ivan Ruchkin. Towards physically interpretable world models: Meaningful weakly supervised representations for visual trajectory prediction. *arXiv preprint arXiv:2412.12870*, 2024.
- [46] Connor Basich, Justin Svegliato, Kyle H. Wray, Stefan Witwicki, Joydeep Biswas, and Shlomo Zilberstein. Competence-Aware Systems. *Artificial Intelligence*, page 103844, December 2022. ISSN 0004-3702. doi: 10.1016/j.artint.2022.103844. URL <https://www.sciencedirect.com/science/article/pii/S0004370222001849>.
- [47] Aniketh Ramesh, Rustam Stolkin, and Manolis Chiu. Robot vitals and robot health: Towards systematically quantifying runtime performance degradation in robots under adverse conditions. *IEEE Robotics and Automation Letters*, 7(4): 10729–10736, 2022. doi: 10.1109/LRA.2022.3192612.
- [48] Alvika Gautam, Tim Whiting, Xuan Cao, Michael A. Goodrich, and Jacob W. Crandall. A method for designing autonomous robots that know their limits.

- In *2022 International Conference on Robotics and Automation (ICRA)*, pages 121–127, 2022. doi: 10.1109/ICRA46639.2022.9812030.
- [49] Nicholas Conlon, Daniel Szafir, and Nisar Ahmed. “I’m Confident This Will End Poorly”: Robot Proficiency Self-Assessment in Human-Robot Teaming. In *2022 IEEE/RSJ International Conference on Intelligent Robots and Systems (IROS)*, pages 2127–2134, October 2022. doi: 10.1109/IROS47612.2022.9981653. ISSN: 2153-0866.
- [50] Jose G. Moreno-Torres, Troy Raeder, Rocío Alaiz-Rodríguez, Nitesh V. Chawla, and Francisco Herrera. A unifying view on dataset shift in classification. *Pattern Recognition*, 45(1):521–530, 2012. ISSN 0031-3203. doi: <https://doi.org/10.1016/j.patcog.2011.06.019>. URL <https://www.sciencedirect.com/science/article/pii/S0031320311002901>.
- [51] Xiaowei Huang, Daniel Kroening, Wenjie Ruan, James Sharp, Youcheng Sun, Emese Thamo, Min Wu, and Xinping Yi. A survey of safety and trustworthiness of deep neural networks: Verification, testing, adversarial attack and defence, and interpretability. *Computer Science Review*, 37:100270, 2020. ISSN 1574-0137. doi: <https://doi.org/10.1016/j.cosrev.2020.100270>. URL <https://www.sciencedirect.com/science/article/pii/S1574013719302527>.
- [52] Radoslav Ivanov, Taylor Carpenter, James Weimer, Rajeev Alur, George Pappas, and Insup Lee. Verisig 2.0: Verification of Neural Network Controllers Using Taylor Model Preconditioning. In *Computer Aided Verification*, pages 249–262, Cham, 2021. Springer International Publishing. ISBN 978-3-030-81685-8.
- [53] Hoang-Dung Tran, Weiming Xiang, and Taylor T. Johnson. Verification Approaches for Learning-Enabled Autonomous Cyber-Physical Systems. *IEEE Design & Test*, 39(1):24–34, February 2022. ISSN 2168-2364. doi: 10.1109/MDAT.2020.3015712. Conference Name: IEEE Design & Test.
- [54] Ulices Santa Cruz and Yasser Shoukry. NNlander-VeriF: A Neural Network Formal Verification Framework for Vision-Based Autonomous Aircraft Landing. In Jyotirmoy V. Deshmukh, Klaus Havelund, and Ivan Perez, editors, *NASA Formal Methods*, Lecture Notes in Computer Science, pages 213–230, Cham, 2022. Springer International Publishing. ISBN 978-3-031-06773-0.
- [55] Chiao Hsieh, Yangge Li, Dawei Sun, Keyur Joshi, Sasa Misailovic, and Sayan Mitra. Verifying Controllers With Vision-Based Perception Using Safe Approximate Abstractions. *IEEE Transactions on Computer-Aided Design of Integrated Circuits and Systems*, 41(11):4205–4216, November 2022. ISSN 1937-4151. doi: 10.1109/TCAD.2022.3197508. Conference Name: IEEE Transactions on Computer-Aided Design of Integrated Circuits and Systems.
- [56] Yahan Yang, Ramneet Kaur, Souradeep Dutta, and Insup Lee. Interpretable Detection of Distribution Shifts in Learning Enabled Cyber-Physical Systems.

In *2022 ACM/IEEE 13th International Conference on Cyber-Physical Systems (ICCPS)*, pages 225–235, May 2022. doi: 10.1109/ICCPS54341.2022.00027.

- [57] Matthew Cleaveland, Lars Lindemann, Radoslav Ivanov, and George J. Pappas. Risk verification of stochastic systems with neural network controllers. *Artificial Intelligence*, 313:103782, December 2022. ISSN 0004-3702. doi: 10.1016/j.artint.2022.103782. URL <https://www.sciencedirect.com/science/article/pii/S0004370222001229>.
- [58] Mojtaba Zarei, Yu Wang, and Miroslav Pajic. Statistical verification of learning-based cyber-physical systems. In *Proceedings of the 23rd International Conference on Hybrid Systems: Computation and Control, HSCC '20*, New York, NY, USA, 2020. Association for Computing Machinery. ISBN 9781450370189. doi: 10.1145/3365365.3382209. URL <https://doi.org/10.1145/3365365.3382209>.
- [59] Xin Qin, Yuan Xia, Aditya Zutshi, Chuchu Fan, and Jyotirmoy V. Deshmukh. Statistical verification of cyber-physical systems using surrogate models and conformal inference. In *2022 ACM/IEEE 13th International Conference on Cyber-Physical Systems (ICCPS)*, pages 116–126, 2022. doi: 10.1109/ICCPS54341.2022.00017.
- [60] Rhiannon Michelmore, Matthew Wicker, L. Laurenti, L. Cardelli, Y. Gal, and Marta Kwiatkowska. Uncertainty Quantification with Statistical Guarantees in End-to-End Autonomous Driving Control. *2020 IEEE International Conference on Robotics and Automation (ICRA)*, 2020. doi: 10.1109/ICRA40945.2020.9196844.
- [61] Craig Knuth, Glen Chou, Necmiye Ozay, and Dmitry Berenson. Planning With Learned Dynamics: Probabilistic Guarantees on Safety and Reachability via Lipschitz Constants. *IEEE Robotics and Automation Letters*, PP:1–1, March 2021. doi: 10.1109/LRA.2021.3068889.
- [62] Michael Hibbard, Abraham P. Vinod, Jesse Quattrociocchi, and Ufuk Topcu. Safely: Safe Stochastic Motion Planning Under Constrained Sensing via Duality, March 2022. URL <http://arxiv.org/abs/2203.02816>. arXiv:2203.02816 [cs, eess].
- [63] Glen Chou and Russ Tedrake. Synthesizing Stable Reduced-Order Visuomotor Policies for Nonlinear Systems via Sums-of-Squares Optimization, September 2023. URL <http://arxiv.org/abs/2304.12405>. arXiv:2304.12405 [cs, eess, math].
- [64] Aaron D. Ames, Samuel Coogan, Magnus Egerstedt, Gennaro Notomista, Koushil Sreenath, and Paulo Tabuada. Control Barrier Functions: Theory and Applications. In *2019 18th European Control Conference (ECC)*, pages 3420–3431, June 2019. doi: 10.23919/ECC.2019.8796030.
- [65] Wei Xiao, Christos G. Cassandras, and Calin Belta. *Safe Autonomy with Control Barrier Functions: Theory and Applications*. Synthesis Lectures on

- Computer Science. Springer International Publishing, Cham, 2023. ISBN 978-3-031-27575-3 978-3-031-27576-0. doi: 10.1007/978-3-031-27576-0. URL <https://link.springer.com/10.1007/978-3-031-27576-0>.
- [66] Sarah Dean, Andrew Taylor, Ryan Cosner, Benjamin Recht, and Aaron Ames. Guaranteeing Safety of Learned Perception Modules via Measurement-Robust Control Barrier Functions. In *Proceedings of the 2020 Conference on Robot Learning*, pages 654–670. PMLR, October 2021. URL <https://proceedings.mlr.press/v155/dean21a.html>. ISSN: 2640-3498.
- [67] Shuo Yang, George J. Pappas, Rahul Mangharam, and Lars Lindemann. Safe Perception-Based Control under Stochastic Sensor Uncertainty using Conformal Prediction. In *CDC 2023*. arXiv, August 2023. arXiv:2304.00194 [cs, eess].
- [68] John C. Platt. Probabilistic Outputs for Support Vector Machines and Comparisons to Regularized Likelihood Methods. In *Advances in Large Margin Classifiers*, pages 61–74. MIT Press, 1999.
- [69] Bianca Zadrozny and Charles Elkan. Transforming classifier scores into accurate multiclass probability estimates. In *Proceedings of the eighth ACM SIGKDD international conference on Knowledge discovery and data mining, KDD '02*, pages 694–699, New York, NY, USA, July 2002. Association for Computing Machinery. ISBN 978-1-58113-567-1. doi: 10.1145/775047.775151. URL <https://dl.acm.org/doi/10.1145/775047.775151>.
- [70] Mahdi Pakdaman Naeni, Gregory F. Cooper, and Milos Hauskrecht. Obtaining Well Calibrated Probabilities Using Bayesian Binning. *Proceedings of the AAAI Conference on Artificial Intelligence*, 2015:2901–2907, January 2015. ISSN 2159-5399.
- [71] Jize Zhang, Bhavya Kailkhura, and T. Yong-Jin Han. Mix-n-Match: ensemble and compositional methods for uncertainty calibration in deep learning. In *Proceedings of the 37th International Conference on Machine Learning, ICML'20*, pages 11117–11128. JMLR.org, July 2020.
- [72] Kimin Lee, Honglak Lee, Kibok Lee, and Jinwoo Shin. Training Confidence-calibrated Classifiers for Detecting Out-of-Distribution Samples. February 2018. URL <https://openreview.net/forum?id=ryiAv2xAZ>.
- [73] Terrance DeVries and Graham W. Taylor. Learning Confidence for Out-of-Distribution Detection in Neural Networks, February 2018. URL <http://arxiv.org/abs/1802.04865>. arXiv:1802.04865 [cs, stat].
- [74] Chen Xing, Sercan Arik, Zizhao Zhang, and Tomas Pfister. Distance-Based Learning from Errors for Confidence Calibration. In *In Proc. of International Conference on Learning Representations*, September 2019. URL <https://openreview.net/forum?id=BJeB5hVtvB>.

- [75] Charles Corbiere, Nicolas Thome, Avner Bar-Hen, Matthieu Cord, and Patrick Perez. Addressing Failure Prediction by Learning Model Confidence. In *Advances in Neural Information Processing Systems*, volume 32. Curran Associates, Inc., 2019. URL <https://proceedings.neurips.cc/paper/2019/hash/757f843a169cc678064d9530d12a1881-Abstract.html>.
- [76] Vladimir Vovk, Ivan Petej, Paolo Toccaceli, Alexander Gammerman, Ernst Ahlberg, and Lars Carlsson. Conformal calibrators. In *Proceedings of the Ninth Symposium on Conformal and Probabilistic Prediction and Applications*, pages 84–99. PMLR, August 2020. URL <https://proceedings.mlr.press/v128/vovk20a.html>. ISSN: 2640-3498.
- [77] Charles Marx, Shengjia Zhao, Willie Neiswanger, and Stefano Ermon. Modular Conformal Calibration. In *Proceedings of the 39th International Conference on Machine Learning*, pages 15180–15195. PMLR, June 2022. URL <https://proceedings.mlr.press/v162/marx22a.html>. ISSN: 2640-3498.
- [78] Matthew Cleaveland, Oleg Sokolsky, Insup Lee, and Ivan Ruchkin. Conservative Safety Monitors of Stochastic Dynamical Systems. In *Proc. of the NASA Formal Methods Conference*, May 2023.
- [79] Sergiu Oprea, Pablo Martinez-Gonzalez, Alberto Garcia-Garcia, John Alejandro Castro-Vargas, Sergio Orts-Escolano, Jose Garcia-Rodriguez, and Antonis Argyros. A review on deep learning techniques for video prediction. *IEEE Transactions on Pattern Analysis and Machine Intelligence*, 44(6):2806–2826, jun 2022. doi: 10.1109/tpami.2020.3045007. URL <https://doi.org/10.1109/2Ftpami.2020.3045007>.
- [80] Junhyuk Oh, Xiaoxiao Guo, Honglak Lee, Richard L Lewis, and Satinder Singh. Action-conditional video prediction using deep networks in atari games. *Advances in neural information processing systems*, 28, 2015.
- [81] Chelsea Finn and Sergey Levine. Deep visual foresight for planning robot motion. In *2017 IEEE international conference on robotics and automation (ICRA)*, pages 2786–2793. IEEE, 2017.
- [82] Mark Strickland, Georgios Fainekos, and Heni Ben Amor. Deep predictive models for collision risk assessment in autonomous driving, 2018.
- [83] Ian Goodfellow, Jean Pouget-Abadie, Mehdi Mirza, Bing Xu, David Warde-Farley, Sherjil Ozair, Aaron Courville, and Yoshua Bengio. Generative adversarial networks. *Communications of the ACM*, 63(11):139–144, 2020.
- [84] Sydney M. Katz, Anthony L. Corso, Christopher A. Strong, and Mykel J. Kochenderfer. Verification of image-based neural network controllers using generative models, 2021.

- [85] Dimitrios Boursinos and Xenofon Koutsoukos. Assurance monitoring of learning-enabled cyber-physical systems using inductive conformal prediction based on distance learning. *AI EDAM*, 35(2):251–264, May 2021. ISSN 0890-0604, 1469-1760. Publisher: Cambridge University Press.
- [86] David Ha and Jürgen Schmidhuber. Recurrent World Models Facilitate Policy Evolution. In *Advances in Neural Information Processing Systems*, volume 31, 2018.
- [87] Aastha Acharya, Rebecca Russell, and Nisar R. Ahmed. Competency Assessment for Autonomous Agents using Deep Generative Models. In *2022 IEEE/RSJ International Conference on Intelligent Robots and Systems (IROS)*, pages 8211–8218, October 2022. doi: 10.1109/IROS47612.2022.9981991. ISSN: 2153-0866.
- [88] Aidan Scannell, Mohammadreza Nakhaei, Kalle Kujanpää, Yi Zhao, Kevin Sebastian Luck, Arno Solin, and Joni Pajarinen. Discrete codebook world models for continuous control. *arXiv preprint arXiv:2503.00653*, 2025.
- [89] Aaron Van Den Oord, Oriol Vinyals, et al. Neural discrete representation learning. *Advances in neural information processing systems*, 30, 2017.
- [90] Danijar Hafner, Timothy Lillicrap, Mohammad Norouzi, and Jimmy Ba. Mastering atari with discrete world models, 2022.
- [91] Vincent Micheli, Eloi Alonso, and François Fleuret. Transformers are sample-efficient world models, 2023.
- [92] Vincent Micheli, Eloi Alonso, and François Fleuret. Transformers are sample-efficient world models. *arXiv preprint arXiv:2209.00588*, 2022.
- [93] Philipp Wu, Alejandro Escontrela, Danijar Hafner, Pieter Abbeel, and Ken Goldberg. Daydreamer: World models for physical robot learning. In *Conference on robot learning*, pages 2226–2240. PMLR, 2023.
- [94] Arian Mousakhan, Sudhanshu Mittal, Silvio Galesso, Karim Farid, and Thomas Brox. Orbis: Overcoming challenges of long-horizon prediction in driving world models. *arXiv preprint arXiv:2507.13162*, 2025.
- [95] Aastha Acharya, Rebecca Russell, and Nisar R. Ahmed. Learning to forecast aleatoric and epistemic uncertainties over long horizon trajectories, 2023.
- [96] Zhenjiang Mao, Siqu Dai, Yuang Geng, and Ivan Ruchkin. Zero-shot safety prediction for autonomous robots with foundation world models. *arXiv preprint arXiv:2404.00462*, 2024.

- [97] Andrea Stocco, Michael Weiss, Marco Calzana, and Paolo Tonella. Misbehaviour prediction for autonomous driving systems. In *Proceedings of the ACM/IEEE 42nd international conference on software engineering*, pages 359–371, 2020.
- [98] Baochen Sun and Kate Saenko. Deep coral: Correlation alignment for deep domain adaptation. In *Computer vision–ECCV 2016 workshops: Amsterdam, the Netherlands, October 8–10 and 15–16, 2016, proceedings, part III 14*, pages 443–450. Springer, 2016.
- [99] Mingsheng Long, Yue Cao, Jianmin Wang, and Michael Jordan. Learning transferable features with deep adaptation networks. In *International conference on machine learning*, pages 97–105. PMLR, 2015.
- [100] Yaroslav Ganin, Evgeniya Ustinova, Hana Ajakan, Pascal Germain, Hugo Larochelle, François Laviolette, Mario March, and Victor Lempitsky. Domain-adversarial training of neural networks. *Journal of machine learning research*, 17(59):1–35, 2016.
- [101] Eric Tzeng, Judy Hoffman, Kate Saenko, and Trevor Darrell. Adversarial discriminative domain adaptation. In *Proceedings of the IEEE conference on computer vision and pattern recognition*, pages 7167–7176, 2017.
- [102] Konstantinos Bousmalis, Nathan Silberman, David Dohan, Dumitru Erhan, and Dilip Krishnan. Unsupervised pixel-level domain adaptation with generative adversarial networks. In *Proceedings of the IEEE conference on computer vision and pattern recognition*, pages 3722–3731, 2017.
- [103] Jun-Yan Zhu, Taesung Park, Phillip Isola, and Alexei A Efros. Unpaired image-to-image translation using cycle-consistent adversarial networks. In *Proceedings of the IEEE international conference on computer vision*, pages 2223–2232, 2017.
- [104] Carson Sobolewski, Zhenjiang Mao, Kshitij Vejre, and Ivan Ruchkin. Generalizable image repair for robust visual autonomous racing. *arXiv preprint arXiv:2503.05911*, 2025.
- [105] Dequan Wang, Evan Shelhamer, Shaoteng Liu, Bruno Olshausen, and Trevor Darrell. Tent: Fully test-time adaptation by entropy minimization. *arXiv preprint arXiv:2006.10726*, 2020.
- [106] Guoliang Kang, Lu Jiang, Yi Yang, and Alexander G Hauptmann. Contrastive adaptation network for unsupervised domain adaptation. In *Proceedings of the IEEE/CVF conference on computer vision and pattern recognition*, pages 4893–4902, 2019.
- [107] Marvin Zhang, Sergey Levine, and Chelsea Finn. Memo: Test time robustness via adaptation and augmentation. *Advances in neural information processing systems*, 35:38629–38642, 2022.

- [108] Volodymyr Mnih, Koray Kavukcuoglu, David Silver, Andrei A Rusu, Joel Veness, Marc G Bellemare, Alex Graves, Martin Riedmiller, Andreas K Fidjeland, Georg Ostrovski, et al. Human-level control through deep reinforcement learning. *nature*, 518(7540):529–533, 2015.
- [109] Ahmed Hussein, Mohamed Medhat Gaber, Eyad Elyan, and Chrisina Jayne. Imitation Learning: A Survey of Learning Methods. *ACM Computing Surveys*, 50(2):21:1–21:35, April 2017. ISSN 0360-0300. doi: 10.1145/3054912. URL <https://doi.org/10.1145/3054912>.
- [110] Mike Schuster and Kuldip K. Paliwal. Bidirectional Recurrent Neural Networks. *IEEE Transactions on Signal Processing*, 45(11):2673–2681, Nov 1997. doi: 10.1109/78.650093.
- [111] Ashish Vaswani, Noam Shazeer, Niki Parmar, Jakob Uszkoreit, Llion Jones, Aidan N. Gomez, Lukasz Kaiser, and Illia Polosukhin. Attention Is All You Need. *arXiv:1706.03762 [cs]*, December 2017. URL <http://arxiv.org/abs/1706.03762>. arXiv: 1706.03762.
- [112] Tian Yu Liu, Matthew Trager, Alessandro Achille, Pramuditha Perera, Luca Zancato, and Stefano Soatto. Meaning representations from trajectories in autoregressive models. *arXiv preprint arXiv:2310.18348*, 2023.
- [113] Cheng Wang. Calibration in deep learning: A survey of the state-of-the-art. *arXiv preprint arXiv:2308.01222*, 2023.
- [114] W Brier Glenn et al. Verification of forecasts expressed in terms of probability. *Monthly weather review*, 78(1):1–3, 1950.
- [115] Jing Lei, Max G’Sell, Alessandro Rinaldo, Ryan J Tibshirani, and Larry Wasserman. Distribution-free predictive inference for regression. *Journal of the American Statistical Association*, 113(523):1094–1111, 2018.
- [116] Chuchu Fan, Xin Qin, Yuan Xia, Aditya Zutshi, and Jyotirmoy Deshmukh. Statistical verification of autonomous systems using surrogate models and conformal inference. *arXiv preprint arXiv:2004.00279*, 2020.
- [117] Greg Brockman, Vicki Cheung, Ludwig Pettersson, Jonas Schneider, John Schulman, Jie Tang, and Wojciech Zaremba. OpenAI Gym, June 2016. URL <http://arxiv.org/abs/1606.01540>. arXiv:1606.01540 [cs].
- [118] Burr Settles. Active learning literature survey. *University of Wisconsin-Madison Department of Computer Sciences*, 2009.
- [119] Alexander Ratner, Stephen H Bach, Henry Ehrenberg, Jason Fries, Sen Wu, and Christopher Ré. Snorkel: Rapid training data creation with weak supervision. *Proceedings of the VLDB Endowment*, 11(3):269–282, 2017.

- [120] Alexander Ratner, Braden Hancock, Jared Dunnmon, Frederic Sala, Shreyash Pandey, and Christopher Ré. Snorkel drybell: A case study in deploying weak supervision at industrial scale. In *Proceedings of the 2019 International Conference on Management of Data*, pages 362–375, 2019.
- [121] Song Wen, Hao Wang, and Dimitris Metaxas. Social ODE: Multi-agent Trajectory Forecasting with Neural Ordinary Differential Equations. In *Computer Vision – ECCV 2022*, Lecture Notes in Computer Science, pages 217–233, Cham, 2022. Springer Nature Switzerland. ISBN 978-3-031-20047-2. doi: 10.1007/978-3-031-20047-2_13.
- [122] Christopher Hahn, Frederik Schmitt, Julius Blechert Tillman, Niklas Metzger, Julian Siber, and Bernd Finkbeiner. Teaching temporal logics to neural networks. In *International Conference on Learning Representations (ICLR)*, 2021.